INVESTIGATION INTO THE DEVELOPMENT AND FUNCTION OF THE GASTROINTESTINAL TRACT OF ZEBRAFISH

A Thesis
by
SAVANNA SHERIDAN

Submitted to the School of Graduate Studies
at Appalachian State University
in partial fulfillment of the requirements for the degree of
MASTER OF SCIENCE

December 2020
Department of Biology

INVESTIGATION INTO THE DEVELOPMENT AND FUNCTION OF THE GASTROINTESTINAL TRACT OF ZEBRAFISH

A Thesis
by
SAVANNA SHERIDAN
December 2020

APPROVED BY:

Mary D. Kinkel, Ph.D.
Chairperson, Thesis Committee

Andrew C. Bellemer, Ph.D.
Member, Thesis Committee

Mark E. Venable, Ph.D.
Member, Thesis Committee

Zack E. Murrell, Ph.D.
Chairperson, Department of Biology

Michael J. McKenzie, Ph.D.
Dean, Cratis D. Williams School of Graduate Studies

Abstract

INVESTIGATION INTO THE DEVELOPMENT AND FUNCTION OF THE GASTROINTESTINAL TRACT OF ZEBRAFISH

Savanna Sheridan
B.A., Appalachian State University
M.S., Appalachian State University

Chairperson: Mary D. Kinkel, Ph.D.

This study aimed to further elucidate how the gastrointestinal tract of zebrafish functions to better utilize the zebrafish model for studying intestinal motility disorders in humans. Zebrafish share a high percentage of genes with humans and have similar yet more simplistic gastrointestinal morphology allowing for relatively simple experimental designs. An assay that allows for the comparison of healthy motility and altered motility was developed. Using the intestinal transit assay that I developed with other lab members, I found that it takes approximately four hours for nine days post fertilization (dpf) larval zebrafish to empty their intestinal bulb when kept under normal conditions. Using trans-cinnamaldehyde as a *trpa1a* agonist, I was able to determine that activation of *trpa1a* increased the intestinal transit rate in 9 dpf zebrafish. In the absence of other nutrients and using Nile red as a tracer, trans-cinnamaldehyde was sufficient to increase the intestinal transit rate. In future studies, the Kinkel lab aims to spatiotemporally map *kita*, *ano1*, *trpa1a*, and *trpa1b* to gain a better understanding of the ion channels and receptors that regulate proper intestinal motility. The zebrafish model may provide potential targets for therapeutics for various intestinal motility disorders.

Acknowledgments

I would like to thank everyone who assisted with this research. I would like to give a special thanks to my advisor, committee, and the other students of the Kinkel lab for their support and contribution: Dr. Mary D. Kinkel, Dr. Andrew C. Bellemer, Dr. Mark E. Venable, Kitt Franse, Hollyn Franklyn, Alena Norton, Tierney Daw, Latanya Gordon, Daniel Lauffenburger, Caleb Lombard, and Lexie Balsiger. I would like to thank my fellow graduate students who were there for me every step of the way. Thank you to Monique Eckerd and everyone from Z-CORE who assisted with taking care of the zebrafish used for this study.

This work was supported by the Biology Department at Appalachian State University, a Travel OSR Grant from the Office of Student Research, and a Graduate Student Association Senate (GSAS) Research Materials Grant from the Cratis D. Willaims Graduate School. I received the Graduate Research Assistant Mentee (GRAM) award from the Cratis D. Williams Graduate School thanks to the hard work and dedication of my advisor, Dr. Mary Kinkel.

Table of Contents

List of Tables

List of Figures

Introduction

Millions of Americans are impacted by a multitude of intestinal motility disorders including Hirschsprung's disease, chronic intestinal pseudo-obstruction (CIP), and inflammatory bowel disease (Burns, 2007; Parkman and Doma, 2006). While some intestinal disorders have effective treatments that is not the case for all of them. Clinical studies have linked a decrease in the number of interstitial cells of Cajal (ICC) to patients dealing with CIP (Jain et al., 2003). Further defining the role of ICC and the genes involved in their development and function will hopefully lead to new treatments.

Many studies have been conducted examining the development of the enteric nervous system (ENS), intestinal smooth muscle (iSM), and interstitial cells of Cajal (ICCs). Zebrafish provide a model system for studying the cells involved in proper intestinal motility. It is already known that zebrafish have ~70% orthologous genes with humans and a similar but more simplistic layout of the intestinal wall, making them ideal model systems (Figure 1) (Howe et al., 2013; Wallace et al., 2005). Of disease-associated genes in humans, zebrafish share ~85%, making them good models for studying pathology (Howe et al., 2013). There are mutant lines of zebrafish that have been shown to mimic Hirschsprung's disease and CHARGE syndrome on a cellular and behavioral level (Cloney et al., 2018; Heanue et al., 2016). While recent studies have made strides in elucidating how intestinal motility in zebrafish develops, there are still many gaps in the knowledge.

About intestinal development and experimental design in different model species

In mammals, it is known that the iSM is controlled by signals from the ENS and ICC (Roberts et al., 2010). The ENS is located in the gastrointestinal (GI) tract and is known to be

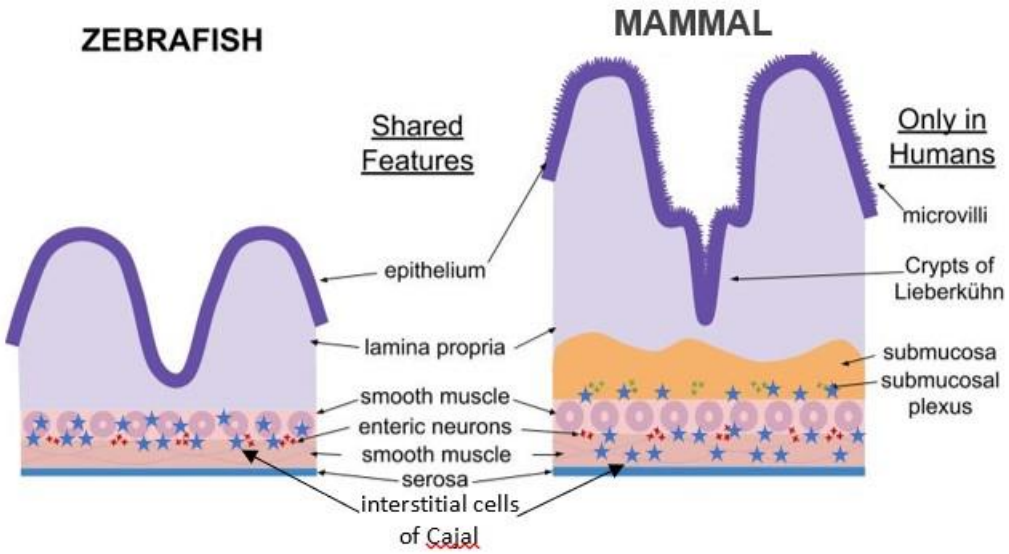

Figure 1. A comparison of structures and cell types in the zebrafish and mammalian intestinal wall. Modified from Franse (2018).

required for proper intestinal motility (Roberts et al., 2010). ICCs are the pacemaker cells of the intestines and are proposed to relay messaged from the ENS to the iSM. The ENS is composed of a myenteric plexus and a submucosal plexus. The myenteric plexus is located between the smooth muscle layers of the intestine and the submucosal plexus is located within the submucosa of the intestinal wall (Figure 1). The ENS signals to the iSM without input from the central nervous system (Olden et al., 2008). By developmental week 14 in humans, a network of ICC is present in close proximity to the myenteric nerve plexus, and the circular and longitudinal smooth muscle layers have formed (Wallace and Burns, 2005). By week 11 myenteric ganglia are observed in the outer layer of longitudinal smooth muscle (Wallace and Burns, 2005).

Mice, chickens, and zebrafish have been used as model organisms to investigate the maturation of intestinal motility. In mice and chickens, oral gavage has been used in

experiments to control the amount of content delivered to the GI tract (Padmanabhan et al., 2013). The timing of intestinal transit can be measured by tracking how long it takes the contents from the oral gavage to be excreted from the mice by using different dyes. Using single-photon emission compute tomography with labeled active charcoal, the movement of the intestinal contents can be tracked through the GI tract *in vivo,* which allows for a more in-depth analysis of intestinal transit (Padmanabhan et al., 2013). However, these methods do not feed the organisms their normal diet, which could be a confounding factor when analyzing the data.

For chicks and mice, the intestines can also be dissected out and placed in an organ bath for mechanical studies. However, these studies can be difficult to conduct after a certain developmental timepoint due to the thickness of the tissue preventing enough oxygen saturation (Chevalier et al., 2019). In mice, it appears that the development of intestinal motility occurs in an anterior-to-posterior pattern (Roberts et al., 2010). In both mice and chicks, the first intestinal motility observed appears to be myogenic meaning the contractions originate within the iSM (Chevalier et al., 2017; Roberts et al., 2010). In mice on embryonic day 13.5 (E13.5) myogenic patterned contractions traveling in both directions are seen in the duodenum but they are not observed in the colon until E14.5 (Roberts et al., 2010). In the mature GI tract, some retrograde contractions occur (Sarna, 2010). However, most contractions are anterograde (Sarna, 2010). Myogenic patterned contractions have an irregular pattern whereas neurogenic patterned contractions are rhythmic. Neurally mediated contractions in mice appear later at E18.5 (Roberts et al., 2010). In chicks, on E12 contraction waves are observed in the circular smooth muscle and by E14 contractions were

seen in the longitudinal smooth muscle (Chevalier et al., 2019). The onset of contractions appears to occur shortly after the iSM has differentiated (Chevalier et al., 2019).

Zebrafish provide an *in vivo* model for tracking intestinal transit time. Since the body wall of zebrafish is transparent when they are young, they allow for more specific time points of digestion and excretion to be tracked when compared to the other models. For example, the time it takes the intestinal bulb to empty versus the mid-intestine to empty could be tracked more readily in zebrafish. In zebrafish, techniques like gut transit assays and live video imaging are used to study the development and function of intestinal motility (Ganz et al., 2018; Holmberg et al., 2007; Uyttebroek et al., 2016). Field et al. (2009) used fluorescently tagged polystyrene microspheres mixed with dry food to track intestinal transit. However, the results of this study were highly variable, likely due to the indigestible material and variance in how much each fish consumed. New techniques to further and more accurately quantify intestinal functionality are being developed using data about the cellular and molecular layout of the intestines of different model organisms.

Timing of the development of intestinal cell types and motility in zebrafish

Using immunohistochemistry, Wallace et al. (2005) found that enteric neurons first differentiated at 72 hours post fertilization (hpf). Antibodies for HuC and HuD were used to stain enteric neurons since they are only expressed in neurons. Formation of the circular smooth muscle layer shortly follows ENS differentiation at 74 hpf but the cells do not appear to be fully differentiated. Using transgenic fish Seiler et al. (2010) found that at around 74

hpf, few precursor cells are observed forming the longitudinal smooth muscle layer. They targeted the gene *sm22α-b* to produce GFP- labeled smooth muscle cells. By 5 dpf (120 hpf), axons of ENS neurons were observed running parallel to the longitudinal smooth muscle (Seiler et al., 2010). According to Seiler et al., (2010), by 6 dpf all iSM appeared fully differentiated (Seiler et al., 2010). At 74 hpf, the intestinal epithelium was highly proliferative and by 120 hpf proliferation exponentially decreased which was observed using BrdU staining (Wallace et al., 2005). This information is summarized in Table 1.

Table 1. Structural development of the gastrointestinal tract.

Event	Timepoints and Description
Epithelium proliferation	Highly proliferative until 74 hpf. Proliferation exponentially decreases by 120 hpf (Wallace et al. 2005).
ENS development	Between 36 and 74 hpf, the enteric neuron progenitors surround the intestinal epithelium (Wallace et al. 2005; Seiler et al. 2010); 5 dpf: ENS axons found in the longitudinal smooth muscle layer parallel to the muscle cells (Seiler et al. 2010).
Smooth muscle differentiation	Between 58 and 72 hpf, smooth muscle progenitor cells migrate and proliferate to populate the entire length of the intestine (Wallace et al. 2005); 72 hpf: Circular smooth muscle forms but appears undifferentiated, some longitudinal smooth muscle is present but is undifferentiated (Seiler et al. 2010). By 144 hpf all smooth muscle cells appear fully differentiated (Seiler et al. 2010)
ICC development	Immunoreactivity of ano1 is first observed at 3 dpf. By 5 dpf a 3D network of ICC is observable when staining with ano1 antibodies (Uyttebroek et al. 2013). Kita immunoreactivity is not observed until 7 dpf (Rich et al. 2013).

Previous studies have examined the functional development of the intestines by measuring the frequency, velocity, amplitude, and distance of contractions. All of the previous studies have measured these parameters in zebrafish with an empty intestinal lumen.

The information from these studies is summarized in Table 2. Spontaneous smooth muscle contractions are first observed at 3.5 dpf (84 hpf) with caudal-to-rostral contractions beginning at 4.5 dpf (108 hpf) (Kuhlman and Eisen, 2007). By 5.5 dpf (132 hpf) rostral-to-caudal contractions appear (Kuhlman and Eisen, 2007). Regular directional contractions appear before exogenous feeding starts (Shepherd and Eisen, 2011). The directional contractions appear 2.5 days prior to the ENS signaling to the iSM, which begins at 7 dpf in zebrafish (Holmberg et al., 2007). This was determined by adding tetrodotoxin (TTX), a

Table 2. Functional development of the gastrointestinal tract.

Movement	**Timepoint and description**
Contraction frequency	More information is needed to determine if frequency changes through development: 4 dpf: 1.03 ± 0.22 and 1.29 ± 0.19 per minute (Holmberg et al., 2007). 6 dpf: 2.24 ± 0.03 per minute (Ganz et al., 2018) 7 dpf: 2.45 ± 0.06 (Ganz et al., 2018) and 1.02 ± 0.13 to 1.07 ± 0.12 (Holmberg et al., 2007).
Contraction distance	Increases from 4 dpf to 7 dpf: 4 dpf: Distance traveled by a contraction was between 543.3 ± 49.6 μm to 638.7± 46.8 μm (Holmberg et al. 2007). 7 dpf: Distance was between 685.1 ± 45.9 μm and 775.6± 37.9 μm
Contraction velocity	Decreases from 4 dpf to 7 dpf: At 4 dpf velocity of contractions were between 49.5 ± 5.5 μm/sec. At 6 dpf the velocity was 42.9 ± 19.3 μm/sec (Ganz et al., 2018). At 7 dpf, the velocity of contractions was between 27.8 ± 3.6 μm/sec (Holmberg et al. 2007).
Contraction direction	Contraction direction matures: Caudal-to-rostral contractions are first observed at 4.5 dpf originating either at the anterior region of the mid-intestine or at the anus (Kuhlman and Eisen, 2007). At 5.5 dpf rostral-to-caudal contractions observed (Kuhlman and Eisen, 2007) Between 5.5- 6.5, dpf contraction waves originating in the intestinal bulb appear peristaltic.

nerve blocker. On 7 dpf, TTX treatment started to have an impact on the duration of

contractions. Specifically, TTX is a voltage-gated sodium channel blocker which blocks neuronal signaling. Based on this information I would predict that the ENS is likely not required for proper peristalsis.

However, since the ENS is specific to the intestines it may be that the ENS can add input to the ICCs and cause the strength of contraction to increase or decrease based on the signals it is receiving. ICCs were not studied directly during these experiments. However, there was some TTX-insensitive activity occurring which could be due to the activity of the ICCs. The velocity of the contractions did not differ between the control group and treatment group on 7 dpf (Holmberg et al., 2007).

Since directionality indicates coordination of contractions at 4.5 dpf, the ICCs are likely signaling to the iSM by 4.5 dpf. Anoctamin1 (ano1) is a channel on the membrane of ICC that is used to label these cells via immunohistochemistry (Uyttebroek et al., 2013). Ano1 reactivity is first observed at 3 dpf (72 hpf) and a full 3-dimensional network of ICC is formed by 5 dpf (120 hpf) (Uyttebroek et al., 2013). The development of the ICC network seems to coincide with the onset of directional contractions which further supports the ICC's role as a pacemaker for intestinal motility. At 3.5 dpf, the spontaneous/nondirectional contractions could either be myogenic or be originating in the developing ICC network. However, kita immunoreactivity is not seen until 7 dpf which is unexpected since kita is thought to be required for the proper development of the pacemaker function of ICC (Rich et al., 2007). Kita is a receptor tyrosine kinase that is known to be a specific marker of ICCs. When c-kit (the mammalian ortholog of kita) was first observed in the intestines, it was found that knocking it down disrupted intestinal motility (Maeda et al., 1992). It could be that ano1 enables the ICC to partially function but that both kita and ano1 are required for the full

function of the ICC to occur. It could also be that ano1 plays a role in the proper development of ICCs as well. More research is needed to determine if the still developing ICC network is able to signal to the iSM and if there is a developmental role for ano1 along with its already known functional role.

Signaling between the different cell types of the gastrointestinal tract

Sanders et al. (2014) have proposed a functional unit called the SIP syncytium to explain how intestinal peristalsis is controlled. This model attempts to explain how multiple intestinal cell types interact to produce proper intestinal motility. The SIP syncytium stands for smooth muscle, interstitial cells of Cajal, and platelet-derived growth factor receptor alpha positive (PDGFR-α^+) cells. These are the core cell types thought to be involved in peristalsis according to the SIP syncytium model. The hypothesis is that instead of the ENS directly signaling to the iSM, it signals to either the ICC and/or to the PDGFR-α^+ cells, which then relay messages to the iSM via gap junctions (Sanders et al., 2014). While there has been a considerable amount of research on the iSM and ICC, the PDGFR-α^+ were first found in the GI tract of mice in 2009 and their function has yet to be elucidated (Iino et al., 2009). PDGFR-α^+ cells are fibroblast-like cells. Due to their proximity to ICCs and enteric neurons, they are proposed to have a functional role in intestinal motility (Iino et al., 2009). These cells are often referred to as fibroblast-like cells and are negative for c-kit immunoreactivity and have not been investigated in the zebrafish GI tract (Iino et al., 2009). In guinea pigs, the gap junction protein connexin 43 and c-kit have been stained in the same regions of intestinal tissue suggesting that ICCs have gap junctions (Cousins et al., 2003). Gap junctions were present between ICC and iSM in the circular smooth muscle layer which

further supports the model proposed by Sanders et al. (2014). The presence of gap junctions supports the idea that the ICC and iSM make up a functional syncytium that allows for regulation of peristalsis. Staining for gap junctions between iSM and ICC has not yet been done in zebrafish.

Intestinal development in zebrafish

In zebrafish studies, techniques such as immunohistochemistry, *in situ* hybridization, gut transit assays, and live video imaging are used to investigate how proper intestinal motility develops. Immunohistochemistry and *in situ* hybridization allow for the timing of developmental events to be studied. These techniques are often paired with mutant lines to understand how specific gene defects impact development (Heanue et al., 2016). In recent studies, mutant lines and live imaging have revealed new insights into the role of *ret* for the development of the ENS and intestinal motility. A better understanding of how different genes impact intestinal development would allow for more target to different intestinal diseases.

Ret is a receptor tyrosine kinase that has been shown to be required for the proper development of the ENS. Since this receptor has been shown to be important in ENS development, *ret* mutants can be used to study intestinal diseases in humans, like Hirschsprung's disease. Heanue et al. (2016) further established zebrafish *ret* mutants as a model by tracking ENS development. They found that in wild-type zebrafish, by 4 dpf the entire GI tract was populated by ENS neurons. However, in homozygous *ret* mutants, ENS neurons were almost absent from the GI tract at 4 dpf. In heterozygotes, neurons were only observed in the rostral mid-intestine. Time-lapse imaging was conducted on the homozygous

and heterozygous *ret* mutants. The zebrafish were embedded in agarose at 48 hpf and imaged for 36 hours to examine the migration of ENS progenitor cells. Typically, zebrafish hatch from the chorions prior to 72 hpf which means they have the ability to swim. This technique requires the zebrafish to be immobilized until 84 hpf which could potentially inhibit healthy development. These experiments indicate that the *ret* gene is necessary for the proper development and migration of enteric neurons (Heanue et al., 2016).

In more recent studies, Ganz et al. (2018) utilized particle image velocimetry (PIV) with spatiotemporal mapping (STMaps) with, what they qualified as, fasted and fed larval zebrafish. PIV takes a set of images and analyzes them to create a set of velocity vectors which can then be used to calculate parameters such as velocity, amplitude, and direction of contractions. Ganz et al. (2018) compared zebrafish that were not fed for three days to those that were fed over those 3 days. However, immediately prior to imaging, zebrafish that had food in the intestinal tract were excluded from the study because the software could not differentiate between movement of the intestinal wall and movement of the gut's luminal contents.

This experiment started at 5 dpf and imaging was conducted through 7 dpf. At 5 dpf, no significant differences were observed in amplitude or frequency between the fasted and unfasted siblings. Considering that zebrafish can have a nutrient-rich yolk sac up to 5 dpf it is not surprising that no differences were observed at this time point. In fed larvae, an increase in the frequency of contraction was observed from 6 dpf to 7 dpf whereas the fasted larvae the frequency remained roughly the same. At 6 dpf the amplitude of contraction was 1.4 times greater in the fed larvae and by 7 dpf the amplitude was 6.5 times greater in the fed larvae. Since this is a crucial time in development, the observations could be a result of

malnutrition in the zebrafish and not necessarily a lack of nutrient reception in the GI tract. Currently, no solution to this issue has been defined.

When comparing the results of similar experiments from Holmberg et al. (2007) some discrepancies can be found. The frequency of contractions observed by Holmberg et al. (2007) at 4 dpf and 7 dpf were both lower than the frequency of contractions observed by Ganz et al. (2018) at 6 dpf and 7 dpf. Each lab used the same general methods for anesthetization and immobilization but used different techniques to analyze the data. Both recorded data for 5 minutes but Ganz et al. recorded 5 frames per second (fps) whereas Holmberg et al. recorded 4 fps. Uyttebroek et al. (2016), however, found very similar contraction frequencies to those of Holmberg et al. (2007). Holmberg et al. (2007) analyzed contraction from the middle of the swim bladder to the anus.

Holmberg et al. only conducted the experiments using zebrafish that had hatched naturally whereas Ganz et al. do not state if this was the case for their procedure. It could be the case that zebrafish that are able to hatch on their own at 3 dpf subsequently grow more quickly than those that do not. Since it has been shown that the post-hatching development of zebrafish more accurately corresponds with the body length of the zebrafish than it does with the age of the fish (Parichy et al., 2009) this difference in experimental procedure could lead to different results.

For these studies, intestinal motility was observed in larval zebrafish with empty intestines. It is known that stretch and nutrients receptors are present in the GI tract, which likely have a role in regulating intestinal motility (Won et al., 2005). By testing fish with empty intestinal lumens instead of fish with contents in the lumen, the way the gut functions in the presence of nutrients and stretch was not being observed. While Field et al. 2008 have

published an intestinal transit assay with a bolus present, they used indigestible polystyrene microspheres which may have impacted intestinal transit time. Therefore, it is important that an intestinal transit assay that provides consistent results and can observe intestinal function with a bolus present in the intestine be developed.

Comparison Between Cardiac Pacemaker Cells and ICC

Cardiac pacemaker cells

Since the pacemaker cells in the heart have been studied more in-depth than the pacemaker cells of the intestines (ICCs) it may be useful to determine the similarities and differences between them. For the heart to function properly and provide blood flow to the entire body it is crucial that the pacemaker cells are functioning correctly. The pacemaker cells in the heart keep the heart muscles contracting in a rhythmic pattern so that blood flow can be continuously provided to the entire body. The electrical pathway of the heart flows from the sinoatrial (SA) node to the atrioventricular (AV) node to the Bundle of His to Bundle branches finally ending with the Purkinje fibers. In a properly functioning heart, the SA node will be the pacemaker (Baruscotti et al., 2010). If the SA node becomes dysfunctional, the AV node becomes the primary pacemaker for the heart (Dobrzynski et al., 2003).

The length of the phases of action potential varies between the working myocytes and the cardiac pacemaker cells. The rate of conduction within the SA and AV node is slower than that of the cardiac myocytes due to the type of connexins that make up the gap junctions they contain (Dobrzynski et al., 2013). This is a consequence of the different ion channels present on the different cell types (Dobrzynski et al., 2013). There are five phases of pacemaking potential: upstroke (phase 0), early repolarization (phase 1), plateau (phase 2),

final repolarization (phase 3), and diastolic depolarization (phase 4) (Figure 2B). The upstroke phase is when the cell voltage rapidly becomes more positive. The early repolarization phase occurs when the peak of depolarization has been reached and rectifying currents become active. The plateau phase is a period when the cell voltage remains relatively constant for a short period after the peak of depolarization is reached. The final repolarization phase ensures that the cell voltage is reset to its resting membrane potential. Finally, diastolic depolarization occurs which activates specific channels necessary for the upstroke.

The pacemaking potential within the SA node is passed on to the AV node via conducting fibers that travel through two pathways in the atria: the terminal crest and the interatrial septum (Meijler and Janse, 1988; Moe et al., 1956; Spach et al., 1971). Summation of the signals from both pathways is needed for the propagation of the signal to continue (Watanabe and Dreifus, 1968). The refractory period, which is a time when another action potential cannot be triggered, within the AV node is relatively long which helps ensure that ventricular contraction does not occur prematurely (Dobrzynski et al., 2013). This allows the ventricles to complete diastole, which is when the heart muscle is relaxed, before systole, or contraction, occurs. Ventricular diastole allows the ventricles to fill with blood. If ventricular diastole was cut short, it would prevent the heart from pumping blood as efficiently as possible, so the refractory period of the AV node plays a crucial role here.

This pattern of contraction is ultimately controlled by a group of autorhythmic cells referred to as pacemaker cells. Autorhythmic cells control the tempo of contraction in the muscle that they signal to. In the heart, there are five main ionic currents that control SA nodal function: Ca^{2+} T-type current (I_{CaT}), Ca^{2+} L-type (I_{CaL}), K^{+} current (I_{K}), funny current

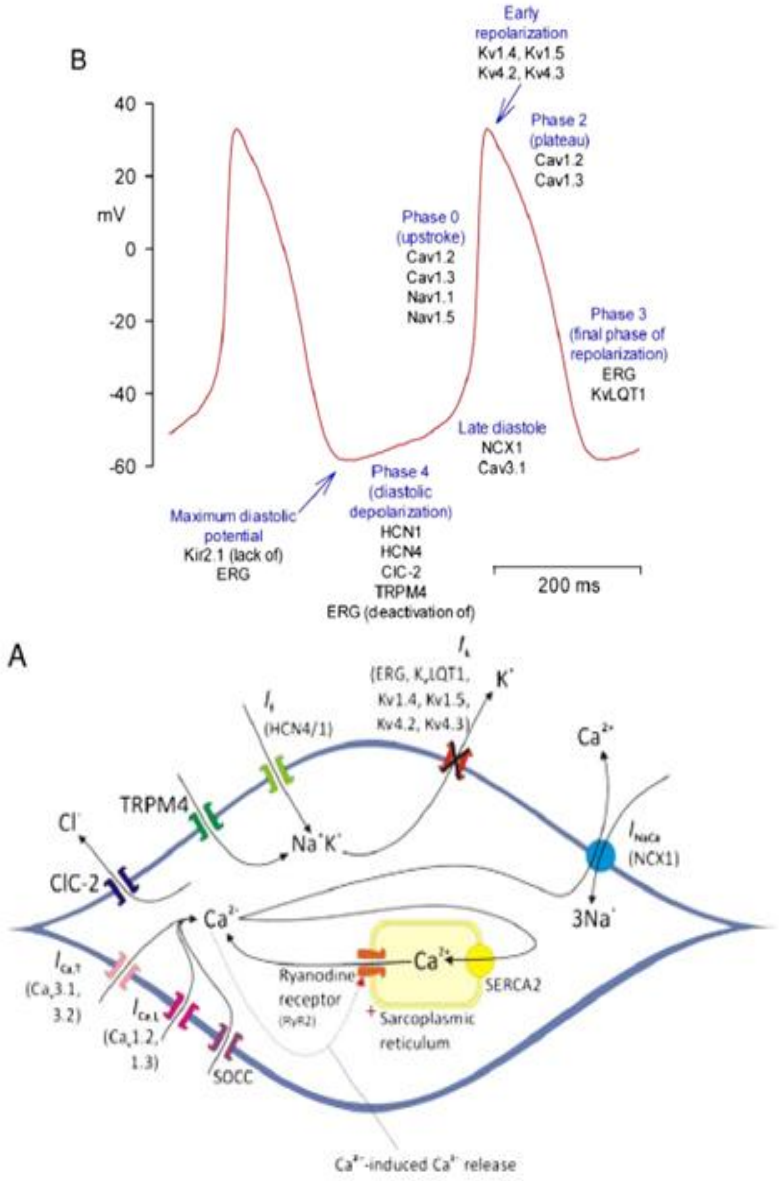

Figure 2. Sinus node pacemaking mechanisms. A) summary of the expression of the main ion channels contributing to the different phases of the nodal action potential. Rabbit sinus node myocyte action potentials shown. B) The multiple ion channels, ionic currents and Ca^{2+}-handling proteins comprising the membrane and Ca^{2+} clocks involved in pacemaking. During the pacemaker potential, there is a voltage-dependent decay of outward currents, $I_{K,r}$ and $I_{K,s}$ (carried by ERG and K_vLQT1), and a voltage-dependent activation of inward currents: I_f (carried by HCN1 and HCN4), Cl^- current (carried by ClC^{-2}), $I_{Ca,L}$ (carried by $Ca_v1.2$ and $Ca_v1.3$) and $I_{Ca,T}$ (carried by $Ca_v3.1$ and $Ca_v3.2$). The Ca^{2+} clock is also involved in pacemaking: there is an activation of inward I_{NaCa} (generated by Na^+–Ca^{2+} exchanger, NCX1) in response to a spontaneous release of Ca^{2+} from the SR via the ryanodine receptor (R_YR2). Ca^{2+} release from the SR also occurs as a result of Ca^{2+}-induced Ca^{2+} release in response to Ca^{2+} entry into the cell via $I_{Ca,L}$ and $I_{Ca,T}$. The SR is replenished with Ca^{2+} by reuptake of Ca^{2+} via SERCA. Store-operated Ca^{2+} channels at the cell surface membrane also help to replenish the sarcoplasmic reticulum with Ca^{2+}. From Dobrzynski et al., 2013.

(I_f), and Na^+/Ca^{2+} current (I_{NaCa}) (Figure 2A). A Na^+ current (I_{Na}) is present but has a much smaller role in the upstroke phase and are not active during the upstroke. Hyperpolarization-activated cyclic nucleotide-gated channel (HCN) 1 and HCN4 are responsible for what is referred to as the funny current (I_f) and are active during diastolic depolarization. These channels open when the cell is hyperpolarized and allow Na^+ and K^+ to move into the cell which causes the membrane potential to become more positive. Hyperpolarization is when the membrane potential becomes more negative than the resting membrane potential. The hyperpolarization-activated channels (HCN1 and HCN4) are active during phase 4 of the pacemaking potential, which is also known as diastolic depolarization (Dobrzynski et al., 2013).

Spontaneous calcium release and reuptake by the sarcoplasmic reticulum via the ryanodine receptor (RYR2) and Sarco/endoplasmic reticulum Ca^{2+} ATPase (SERCA), respectively, control the Ca^{2+} "clock" (Dobrzynski et al., 2013). In other words, this clock is dependent on calcium recycling within the cell (Sherwood and Cengage Learning (Firm), 2013). The main ionic currents in cardiac pacemaking are the funny current and the Ca^{2+} current. Spontaneous release of Ca^{2+} from the sarcoplasmic reticulum triggers activation of the Na^+/Ca^{2+} exchanger 1 (NCX1) during late diastole, right before upstroke (phase 0) begins (Figure 2)(Bogdanov KY. et al., 2001). NCX1 brings 3 Na^+ ions into the cells for everyone 1 Ca^{2+} ion it takes out of the cell. This makes the membrane potential more positive. The rising membrane potential leads to the opening of $Ca_v3.1$ and 3.2 (I_{CaT}) channels during late diastole as phase 4 begins,
which causes an inward Ca^{2+} current (Figure 2). Thus, the spontaneous local influx of Ca^{2+} (from the sarcoplasmic reticulum) induces a larger influx of Ca^{2+} from the extracellular fluid,

resulting in depolarization of the membrane. During the upstroke (phase 0) of the pacemaker potential, $Ca_v1.2$ and 1.3 (I_{CaL}) and $Na_v1.1$ and $Na_v1.5$ channels are activated (Figure 2). $Na_v1.1$ and $Na_v1.5$ play a smaller role in upstroke than $Ca_v1.2$ and $Ca_v1.3$. Since it is mainly I_{CaL} (long-lasting calcium channels) involved in the upstroke of the pacemaker potential, the pacemaker potential upstroke occurs much slower than in the contractile myocardium, which is mainly controlled by I_{Na+} which has a faster and larger conductance (Dobrzynski et al., 2013).

$Ca_v1.3$ is more highly expressed than $Ca_v2.1$ in the AV node than in the cardiac myocytes. Several studies suggest that this is probably because $Ca_v1.3$ has a slightly more negative activation threshold than $Ca_v1.2$ which may make it more suited for pacemaking (Chandler et al., 2009; Greener et al., 2011; Zhang et al., 2000). Once the peak of the pacemaker potential (the most positive voltage) is reached, I_k begins early repolarization (phase 1) by providing an outward K^+ current (Figure 2). The channels active here are $K_v1.4$, $K_v1.5$, $K_v4.2$, and $K_v4.3$. Simultaneously, $Na_v1.1$ and $Na_v1.5$ inactivate but $Ca_v1.2$ and $Ca_v1.3$ remain active through the plateau phase (phase 2). ERG (ether-a-go-go channel) and K_vLQT1 (a voltage-dependent K^+ channel) are responsible for bringing the pacemaker cells back to their resting potential which tends to be around -60 mV. They control what is referred to as the delayed rectifier K^+ current (I_K) (Monfredi et al., 2010). When this process starts again, the ERG is inactivated as HCN1 and HCN4 become active once again.

The speed of conduction in different areas of the heart is also impacted by the type of connexins present. Connexins are the proteins that makeup gap junctions and each type is associated with different speeds of conduction. Gap junctions allow adjacent cells to propagate signals to one another. In the SA node and AV node, the primary connexin (Cx)

expressed is Cx45, which is a small conductance connexin (20-40 pS)(Coppen and Severs, 2002; Coppen et al., 1999). The highest expressed connexin in the working myocardium is Cx43, which has an intermediate conductance (60-100 pS)(Shin Y. et al., 2006) (Shin Y. et al., 2006). This allows for the contraction of the in the ventricles to occur rapidly.

How pacemaker potential results in action potential

Surrounding the SA node is the paranodal area. This is a transitional region is located above the SA node and shares similar ionic channels with both the SA node and the atrial muscle. This region communicates with the atrial muscle so that action potentials, and therefore muscle contraction, occur (Aslanidi et al., 2011). Via both the terminal crest and the interatrial septum, the action potential moves to the AV node. Since Cx45, a low conductance connexin, is the main connexin making up gap junctions in the AV node, and it is expressed at relatively low levels when compared to the ventricular muscle, the action potential moves slowly from pacemaker cell to pacemaker cell within the AV node. The action potential is conducted from the AV node to the atrial muscle via the His-Purkinje system. The Bundle of His branches into the left ventricle and right ventricle leading to Purkinje fibers on both sides of the heart. The Purkinje fibers rapidly conduct the action potential due to an increase in expression of $Na_v1.5$ and the presence of high and medium conductance connexins, Cx40 and Cx43, respectively (Aslanidi et al., 2010; Atkinson et al., 2011; Gourdie et al., 1993). The changes in the expression of both voltage-dependent channels and gap junctions throughout the different cells and tissues within the heart allow for different regions to conduct electrical waves at different times and at different speeds. This system is insulated from the ventricular muscle so that the action potential can be

carried to the apex of the heart and so the ventricular muscle contracts in a highly coordinated, rhythmic pattern.

Evidence that interstitial cells of Cajal are autorhythmic

In 1911 Santiago Ramon y Cajal discovered the cells in the intestinal wall that are now referred to as interstitial cells of Cajal (ICC). He concluded that these cells were a subtype of neurons since the stain he was using was known to stain neurons. However, since these cells were discovered they have been defined as Schwann cells, fibroblasts, and neurons (Thuneberg, 1999). Author Keith in 1915 was the first to propose the branched cells in the myenteric plexus as a pacemaker or nodal-like cells, as seen in the heart (Huizinga et al., 2013). It was not until 1947 that Ambache was able to show evidence that this hypothesis may be correct.

Ambache measured the electrical waves in the intestines and noticed a slow-moving electrical wave that moved through the gut before contractions occurred. Through a series of drug treatments, it was determined that the first electrical wave was not originating in the muscle cells themselves but a network of cells adjacent to the muscle. One very likely possibility proposed were the cells described by Ramon y Cajal which, at the time, were still considered nerve cells (Ambache, 1947).

Faussone-Pelligrini et al. (1977) concluded that these cells were the pacemaker cells based on histological findings using human tissue. They observed many similarities between the ultrastructure of the cardiac pacemaker cells and the ICC such as a plethora of mitochondria and a lack of contractile fibers. Due to the ICC having extensive smooth endoplasmic reticulum (SER) and little rough ER (RER), they ruled out iSM, neurons, and

fibroblasts for the identity of these cells. Although these data supported the hypothesis that ICC are pacemaker cells, it was indirect evidence. Stronger evidence was provided by Suzuki et al. (1986) who observed that a muscle layer lacking the ICC network also lacked the electrical slow wave. These experiments were conducted on the small intestine (jejunum) of cats.

Further evidence regarding the identity of the ICC was provided by experiments showing that in mice lacking an enteric nervous system, slow waves persisted (Ward et al., 1999). Since the electrical slow wave persisted in the absence of neuronal input there must be other cells that they are originating from. When tetrodotoxin, a voltage-gated sodium channel blocker that blocks nerve signaling, was added to the small intestine of a cat, slow electrical waves were still detected (Ohkawa and Watanabe, 1977). By simultaneously recording the mechanical activity of the circular smooth muscle cells (SMC) and the electrical activity of the ICC in between the circular and longitudinal SMC of mice, Yoneda et al. (2004) determined that the contraction of the circular SMC was synchronized with the plateau phase of the ICC slow wave. This synchronicity was not impacted by the nerve blockers tetrodotoxin or atropine. It was these types of experiments that demonstrated that ICCs are not neurons.

Defining the slow wave

The slow wave is an electrical wave that moves through the GI tract prior to the action potential and subsequent contraction of the SMC. It starts in the network of ICC and then is propagated to the SMC via gap junctions (Daniel et al., 1998; Yamamoto, 1977). The slow wave is initiated by a semi-rhythmic release of Ca^{2+} from the ER through the inositol

1,4,5-triphosphate receptor type 1 (IP_3R1) channel within a single ICC (Figure 3). The signal that triggers the release of Ca^{2+} from the ER has not yet been elucidated. This Ca^{2+} release triggers the opening of a calcium-activate chloride channel (CaCC), ano1, on the plasma membrane. Ano1 is highly expressed in ICC (Chen et al., 2007; Zhu et al., 2009). While CaCCs were discovered in salamanders in 1982, it was only in 2008 that ano1 was determined to be a CaCC (Bader et al., 1982; Schroeder et al., 2008; Yang et al., 2008). Opening the ano1 channel allows Cl^- ions to move out of the cell which increases the membrane voltage of the cell (Figure 3). The efflux of Cl^- produces spontaneous transient inward currents (STICs) which in turn leads to spontaneous transient depolarizations (STDs). Once the cell is depolarized, a voltage-dependent Ca^{2+} channel (VDCC) on the cell membrane opens causing an influx of Ca^{2+} leading to more Ca^{2+} being released from the ER (Figure 3). This influx of calcium is what controls the upstroke of the slow wave. This influx of Ca^{2+} into the cytoplasm of a single ICC from the ER and extracellular solution triggers neighboring ICC to depolarize because the cells are electrically coupled via gap junctions (Figure 3) (Cousins et al., 2003; Jiménez et al., 1999). These gap junctions are composed primarily of Cx43, which is a medium conductance connexin (Jiménez et al., 1999). As the Ca^{2+} concentration within a single ICC increases, ions flow through the gap junctions to electrically coupled ICC and cause depolarization, activating the VDCC on their membranes. The reuptake of Ca^{2+} by the Sarco/Endoplasmic Reticulum Ca^{2+}-ATPase (SERCA) pump on the ER membrane causes the end of a slow wave (Figure 3). The wave of muscle contraction follows closely behind the slow wave of the ICC network.

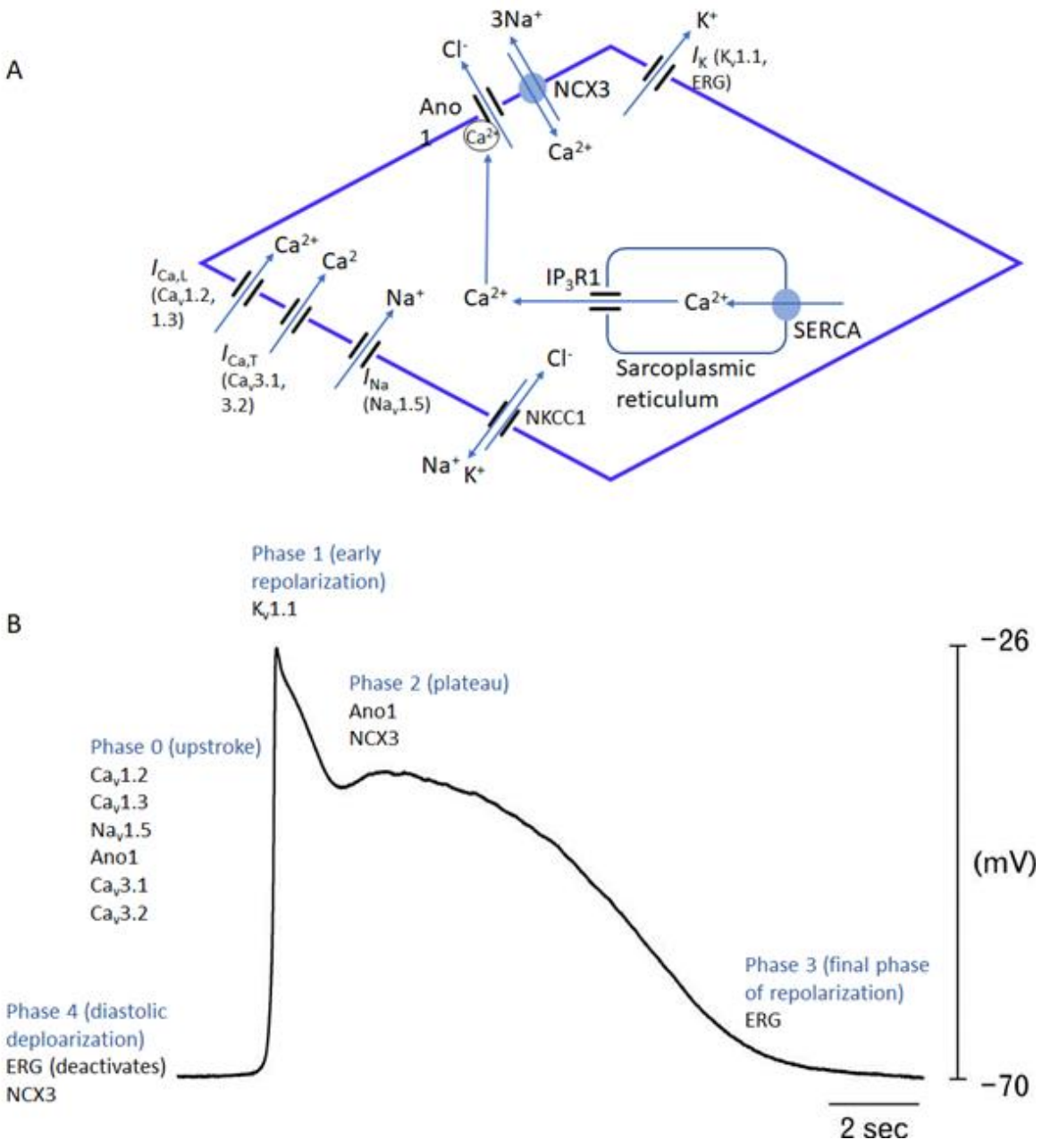

Figure 3. Proposed model of the interstitial cells of Cajal pacemaking mechanism. A) The ion channels and corresponding ionic currents involved in the pacemaking mechanism. During the pacemaker potential, there is a voltage-dependent decay of outward currents, I_k (K_v1.1 and ERG) and a voltage-dependent activation of inward currents: $I_{Ca,L}$ (carried by Ca_v1.2 and Ca_v1.3) and $I_{Ca,T}$ (carried by Ca_v3.1 and Ca_v3.2). The calcium-activated chloride channel ano1 has a high current density during the slow wave. The inward Cl^- replenishes the intracellular Cl^- (carried by NKCC1). The Ca^{2+} clock is also involved in pacemaking: there is an activation of inward I_{NaCa} (generated by Na^+–Ca^{2+} exchanger, NCX3) in response to a spontaneous release of Ca^{2+} from the SR via the IP_3R1. The SR is replenished with Ca^{2+} by reuptake of Ca^{2+} via SERCA. B) Summary of the expression of the main ion channels contributing to the different phases of the ICC slow wave. Data from human gastric antrum myocytes electrical slow wave. (Panel B is modified from Blair et al. 2014)

Comparing ICC slow waves to the slow waves in the cardiac pacemakers

While the heart pacemaker cells are said to be controlled by both a calcium "clock" and voltage "clock", ICCs are proposed to be primarily controlled by a Ca^{2+} "clock" (Joung et al., 2009; Lakatta and DiFrancesco, 2009; Zhu et al., 2009). A model proposed by Sanders et al. (2014) shows that the Ca^{2+} released from the ER first triggers ano1 channels to open which causes depolarization to begin. Then T-type VDCCs open. In ICC, depolarization is what activates the necessary ionic currents for the upstroke phase of the slow wave to occur. However, the intracellular concentration of Ca^{2+} is what controls the slow wave (Zhu et al., 2009). The ICCs propagate the slow wave to the iSM which can lead to action potential occurring in the iSM only. In the heart, the exact process of how diastolic depolarization is triggered is still not yet fully understood (Dobrzynski et al., 2013). This process in the ICC is said to be stochastic but the exact mechanism that is controlling this flow does not appear to be known yet (Blair et al., 2014). Both the ICC and cardiac pacemaker cells have a plateau phase that follows the peak of depolarization but the plateau in ICC is much longer (Dobrzynski et al., 2013; Zheng et al., 2020). The plateau phase in ICC lasts up to several seconds while the cardiac pacemaker plateau lasts ~0.1 seconds (Dobrzynski et al., 2013; Langton et al., 1989). Also, the length of the plateau phase of ICC can vary greatly between different segments of the GI tract and also varies between species (Langton et al., 1989). The longer plateau in ICC is most likely due to the long-lasting activity of ano1. The resting membrane potential of ICC is ~ -65 mV while cells in the SA node do not have a stable resting potential due to the lack of certain K^+ channels (Kito et al., 2002; Koh et al., 1998; Monfredi et al., 2010). The peak voltage of depolarization in the cardiac pacemaker cells is ~35 mV while the peak of depolarization for ICC is roughly between -30 and -10 mV (Figure

2; Figure 3) (Blair et al., 2014; Kito et al., 2005; Koh et al., 1998). The lower peak voltage in ICC must be due to the different activation and inactivation threshold of the voltage-dependent ion channels present on the membrane. In both the ICC and cardiac pacemakers, after the plateau phase repolarization returns the membrane potential back to the start of the slow wave, to begin again. The relatively low peak of the slow wave in ICC is interesting since mainly ion channels and currents that increase the voltage within the cell have been discovered. Therefore, it can be hypothesized that there are key ion channels yet to be identified that are involved in hyperpolarization of ICC or that the expression levels of these channels differ in these cells.

Many channels within ICC are similar to those found in the cardiac pacemaker cells. An isoform of NCX is expressed in cardiac pacemaker cells, NCX1 (Bogdanov KY. et al., 2001). The role NCX1 has in pacemaking of the heart is to remove Ca^{2+} from the cell while bringing Na^{+} into the cell (Figure 2). NCX3 was observed to be closely associated with ano1 on the ICC in the colon of mice (Zheng et al., 2020). However, during slow waves in ICC, it has been proposed that NCX3 channels bring Ca^{2+} into the cell instead of out of the cell, as seen in the heart (Drumm et al., 2015). This contradicts the findings that when the activity of NCX3 is blocked, the Ca^{2+} activated Cl^{-} current increases. The change in the directionality of NCX3 seems to be caused by changes in membrane potential and the ionic gradient throughout the slow wave (Zheng et al., 2020). These findings indicate that NCX3 plays a role in removing Ca^{2+} from the cell (Zheng et al., 2020). If NCX3 is continuously allowing Ca^{2+} into the cell then Ano1 would stay active longer. Due to this, I hypothesize that 1) during slow waves, NCX3 is in Ca^{2+} entry mode; 2) NCX3 and ano1 are

simultaneously active during the plateau phase, for Ca^{2+} influx and Cl- efflux; and 3) when repolarization is occurring, NCX3 shifts to Ca^{2+} efflux mode (Figure 3).

CaCCs are known to have a major role in action potential waveform and ano1 is currently proposed as the main ion channel controlling the pacemaking potential of ICC (Kuruma and Hartzell, 2000; Zhu et al., 2009). When ano1 activity was blocked by niflumic acid, spontaneous slow waves ceased both in intact muscle and in cell culture (Hwang et al., 2009; Zhu et al., 2009). In the heart, HCN1, HCN4, and NCX1 are the main channels that initiate the depolarization (Dobrzynski et al., 2013). Ano1 has not been shown to have any role in the pacemaking potential of cardiac pacemaker cells. It has been shown that $Ca_v1.2$ has a role in proper pacemaking in the GI tract but it has not been determined if these channels have a role in Ca^{2+} transients in ICC (Drumm et al., 2019a; Wegener et al., 2006). In heart pacemaker cells, both $Ca_v1.2$ and $Ca_v1.3$ are present. When Drumm et al. (2019) determined that $Ca_v1.3$ are present on ICC. However, when blockers of $Ca_v1.2$ and $Ca_v1.3$ were added they had no impact on the Ca^{2+} transients. It is likely that either these channels or channels similar to them are present on ICC since their current density is lower than that of Na^+ channels which would contribute to the slower upstroke when compared to the smooth muscle. Through PCR experiments on mouse ICC, it was discovered that $Ca_v3.1$ and $Ca_v3.2$ are expressed which are both T-type Ca^{2+} channels (Zheng et al., 2014). In mice with $Ca_v3.2$ channels knocked out, the upstroke velocity is decreased indicating an essential role for $Ca_v3.2$ in proper pacemaking (Zheng et al., 2014).

Cardiac myocytes, cardiac pacemaker cells, and ICC are repolarized by an outward K^+ current. ICCs express the K^+ channel $K_v1.1$, which has been colocalized with c-kit, indicating its expression on ICC (Hatton et al., 2001). C-kit is a known marker of ICC. In the

heart, the K^+ channels active during early repolarization are $K_v1.4$, $K_v1.5$, $K_v4.2$, and $K_v4.3$ (Dobrzynski et al., 2013). Both in the ICC and the cardiac pacemakers ERG is found (Zhu et al., 2003). In ICCs, when ERG K^+ channels were blocked it was found that the excitability of the tissue increases which is measured by an increase in the slow wave duration (Zhu et al., 2003).

The SCN5A gene was shown to be expressed in human ICC via RT-PCR (Strege et al., 2003). This gene encodes $Na_v1.5$, which is a channel that is known to be also present in cardiac pacemaker cells. $Na_v1.5$ was activated mechanically with stretch in ICC from human jejunum (Strege et al., 2003). When $Na_v1.5$ channels on ICCs were blocked with lidocaine the frequency of the slow wave decreased (Strege et al., 2003). In the heart, this channel is active during the upstroke of the action potential (Monfredi et al., 2010). In the heart mutations of this channel has been shown to result in cardiac arrhythmias and has also been shown to be hereditary (Grant et al., 2002). It has been proposed that mutations found in ion channels within heart pacemaker cells may cause similar pathologies within the GI tract (Lyford and Farrugia, 2003).

A Na^+-K^+-Cl^- cotransporter (NKCC) was shown to have a role in proper intestinal motility (Zhu et al., 2016). Subsequent studies using immunohistochemistry demonstrated that NKCC was present on ICC (Zhu et al., 2016). The role of NKCC in pacemaking in the gut appears to be replenishing the intracellular Cl^- which is essential for the ano1 channel to continue to remove Cl^- from the cell (Zhu et al., 2016). Through a series of drug treatments on ICC from the small intestine of mice it was determined that if NKCC is blocked, pacemakers activity ceases (Youm et al., 2019). There have not been any NKCCs shown to

be important in the cardiac pacemaking potential which indicates no role for ano1 in cardiac pacemaking.

While there are many similarities in the types of channels present on both the ICC and the cardiac pacemakers, the roles of the channels are not always the same. This was seen with the NCX1 in the heart versus the NCX3 in the ICC and the directionality of the ionic gradient. There are many gaps in knowledge for ICC function which makes it difficult to compare with the better-studied cardiac pacemakers. However, our knowledge of the cardiac pacemakers helps to elucidate what studies are needed to acquire a comprehensive picture of how the ICCs generate the slow wave. For example, a full picture of the different ion channels present on ICC would allow for more comprehensive studies for the treatment of gut motility disorders. While numerous studies are being conducted to find treatments for specific GI disorders/diseases, this work is limited by our current lack of understanding of pacemaking in the GI tract.

Anatomically, the pacemaking conduction systems of the heart and GI tract vary greatly. As mentioned earlier, in the heart the electrical wave starts in the sinoatrial (SA) node, flows to the atrioventricular (AV) node, to the bundle of His, to the bundle branches, and ends in the Purkinje fibers. As electrical waves travel through this system, they are insulated from the cardiac myocytes. In the GI tract, the ICC network is found between the circular smooth muscle and longitudinal smooth muscle. Since the ICC and iSM are closely associated throughout the GI tract, it is important to study the tissues as a unit. Gap junctions between ICC and iSM have been observed which likely means that the slow electrical wave is being propagated through the gap junctions. It appears that the ICC network is not insulated from the iSM like the conduction system within the heart is insulated from the

cardiac myocytes. This means that as the slow wave is propagated through the network of ICC the iSM will propagate a slow wave shortly after the adjacent ICC.

Structural and Functional Description of Anoctamin1

TMEM16 protein family members consist of 10 transmembrane proteins that were all originally described as lipid scramblases (Yang et al., 2008). However, it has recently been discovered that TMEM16A and TMEM16B function as Ca^{2+}-activated Cl^- channels (CaCCs) and do not have lipid scramblase activity (Caputo et al., 2008; Schroeder et al., 2008; Yang et al., 2008). TMEM16A has a role in multiple pathologies included breast cancer, stromal GI tumors, and head and neck squamous cell carcinomas (Pedemonte and Galietta, 2014). In mammals and zebrafish, TMEM16A is also known as anoctamin1 (Ano1) (Berg et al., 2012). Anoctamins are known to have roles in neuronal excitability, iSM contraction, and excretion from epithelial cells (Hartzell et al., 2005). In recent years there has been a spike in research investigating Ano1 functional importance in the GI tract, specifically on ICC. The basic structure of ano1 is a double-barreled homodimer with 10 transmembrane domains (TM) per subunit (Le et al., 2019). Whether the channel is in the opened or closed conformation depends on the binding of 2 molecules, PIP_2 and Ca^{2+}. TMEM16A and TMEM16F are currently the only members of the TMEM16 family of proteins that are known to be regulated by PIP_2.

The structure of Ano1

Multiple structural analyses have identified key amino acid residues for the function of TMEM16A. The hourglass-like shape of TMEM16A was determined using cryo-electron

microscopy is shown in Figure 4 (Paulino et al., 2017a). There is a wide intracellular vestibule that allows for Cl^- to enter the pore. The intracellular vestibule also provides Ca^{2+} access to the Ca^{2+} binding sites. The middle region of the pore is referred to as the neck of the pore. At its most narrow point, it is 2.5 Å and ~20 Å long (Paulino et al., 2017b). Then there is the extracellular vestibule that allows the Cl^- to exit the channel.

The overall structure of the Ano1 protein does not differ significantly from other TMEM16 proteins (Paulino et al., 2017a). However, the pore of ano1 differs significantly

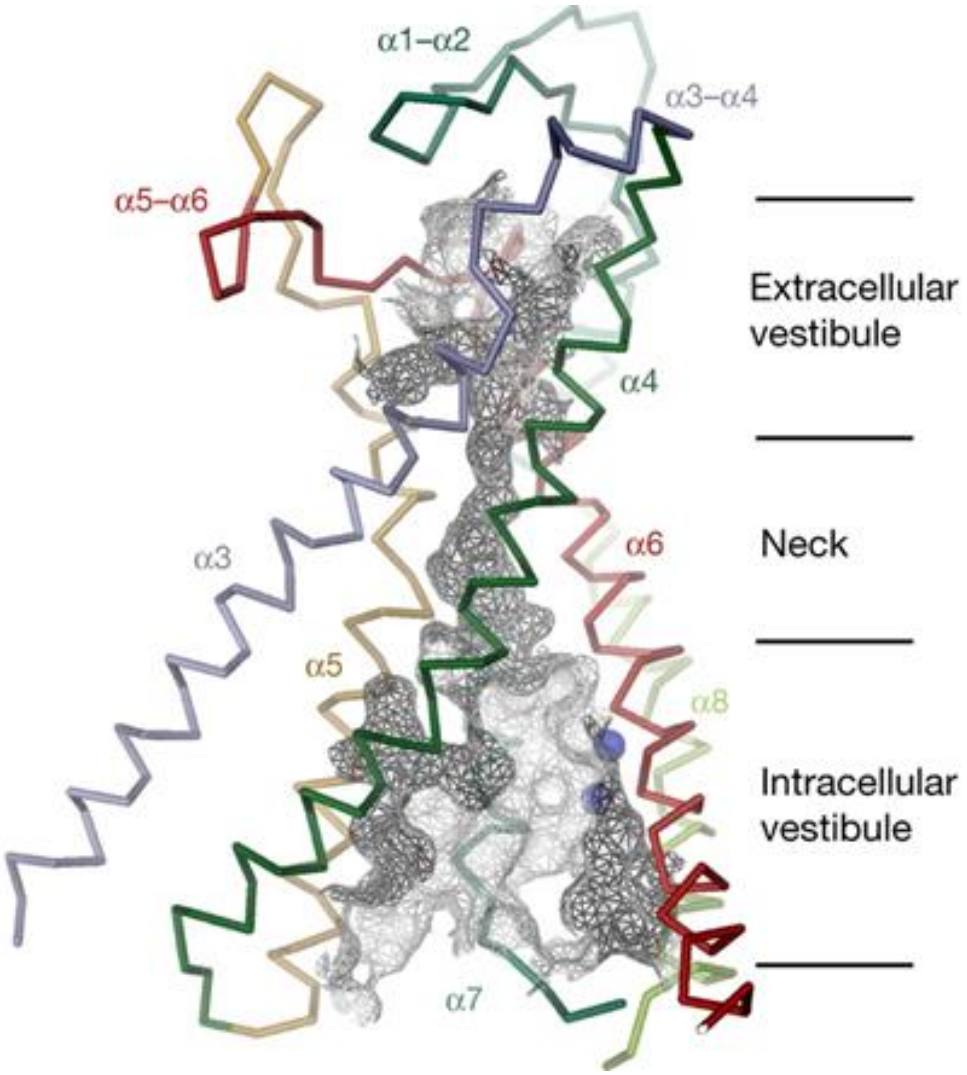

Figure 4. Mouse TMEM16A structure in a Ca^{2+} bound state. The grey mesh shows the ionic conductance pore of the protein. The blue spheres represent Ca^{2+} (Paulino et al. 2017a).

with regard to its functions and its interaction with the hydrophobic layer of the cell membrane (Paulino et al., 2017a). Through cryo-electron microscopy, it was determined that the pore does not have regions that allow for interactions with the lipids in the cell membrane as seen in other TMEM16 proteins (Paulino et al., 2017b). Instead, the neck of the pore is amphiphilic with no charged residues and this allows charged ions such as Cl^- to pass through with relative ease (Paulino et al., 2017b). Specific positive residues on the intracellular and extracellular vestibule of the pore create a positive electrostatic environment that is conducive to attracting anions such as Cl^- (Paulino et al., 2017b). If certain charged amino acids are replaced with neutral amino acids the current of ano1 significantly changes. For example, if arginine is replaced by alanine at the 515^{th} amino acid (R515A) the current-voltage relationship is altered in both directions (Paulino et al., 2017a). From this information, it can be concluded that specific residues are necessary for the energy barrier to be low enough for Cl^- to enter and exit the pore without resistance.

Since this is a Ca^{2+} activated channel, it requires Ca^{2+} in order to shift to an open conformation. Once the channel is triggered to shift to the open conformation Cl^- can pass through. This pathway is modulated by M_3 muscarinic receptors which are expressed on ICC along with ano1 (Sanders et al., 2012). M_3 muscarinic receptors are coupled with $G_{q/11}$ which activates phospholipase C (PLC) (Sanders et al., 2012). When M_3 muscarinic receptors are bound by an agonist, such as acetylcholine, this G-protein coupled pathway is activated (Koh and Rhee, 2013). Activated PLC hydrolyzes phosphatidylinositol 4,5-bisphosphate (PIP_2) into diacylglycerol and inositol-1,4,5-triphosphate (IP_3) (Berridge et al., 2000). IP_3 is the molecule that triggers Ca^{2+} release from the ER by binding IP_3 receptor type 1 (IP_3R1) (Berridge et al., 2000).

Since it is known that Ca^{2+} release from the endoplasmic reticulum (ER) through IP_3R1 is what activates ano1, it could be assumed that activation of M_3 upregulates slow wave activity in ICC (Ward et al., 2000). This pathway requires the presence of PIP_2 which is known to pool within different cellular compartments of the cell (Legate et al., 2012). Supporting this, IP_3R1 staining via immunohistochemistry showed that it colocalizes with ano1 in dorsal root ganglia (Jin et al., 2013). It seems likely that pools of IP_3 would be found in areas where ano1 is present on the plasma membrane if they could be stained together. However, an extensive search of the literature did not find any studies on this. Since IP_3 is diffusible it would be more feasible to stain for PLC since they are known to be found in the same location. Since IP_3R1's substrate is a product of the hydrolysis of PIP_2, it is likely that PIP_2 would also be located in the same region of the cell with ano1. This hypothesis is further supported by the data collected by Yu et al. (2019) and Le et al. (2019) showing that there are binding sites for PIP_2 on ano1. These studies support a model in which this pathway leads to two conformational changes of ano1 in response to Ca^{2+} binding and PIP_2 binding. To determine how ano1 activation is controlled, interactions between phosphatidylinositol 4,5-bisphosphate (PIP_2) binding and ano1 were investigated using HEK293 cells. Yu et al. (2019) engineered different ano1 mutants that replaced basic amino acid residues (lysine and arginine) with a neutral amino acid (glutamine). When the activity of these mutants were compared to the wild type in the presence of dioctanoyl phosphatidylinositol 4,5-bisphosphate (diC_8-PIP_2) 20 mutants recorded a significant reduction in activity (Yu et al., 2019). diC_8-PIP_2 has a shorter acyl chain than PIP_2. Neutralized residues that resulted in >90% reduction in ano1 currents were considered critical and allowed the researchers to define 3 electronegative pockets. To provide more evidence for PIP_2 binding sites on ano1,

molecular dynamic (MD) simulations were utilized. Briefly, molecular dynamic simulations utilize the laws of motion in an algorithm to predict/model how atoms/molecules within a system move and interact (Vlachakis et al., 2014). MD simulation is used to provide higher resolution images for interactions between molecules that experiments cannot. There were eight sites that were observed to interact with PIP_2 and three of those sites accounted for 84.3% of the interactions between PIP_2 and ano1. The sites from MD simulation topographically aligned with the three electronegative pockets identified which indicates that PIP_2 binding is needed for the proper function of ano1. These sites were located on transmembrane domains (TM) 3-5. While MD simulations can pinpoint the exact interactions between PIP_2 and ano1 it requires previous knowledge on the native structure of ano1 in live cells which has not been fully defined yet (Yu et al., 2019). This means that *in vivo* interactions might vary from those observed in MD simulations.

Le et al. (2019) also examined the importance of PIP_2 for ano1 function using HEK293 cells. When ano1 is bound by Ca^{2+} for a prolonged period Ca^{2+} desensitization occurs and ano1 current becomes undetectable after 4-5 mins (Le et al., 2019). In the presence of PIP_2, the strength of the ano1 current was maintained at about half of its initial current after five minutes of activation and becomes undetectable around 7.5 minutes. These results indicated that PIP_2 binding to ano1 attenuates Ca^{2+} desensitization since in the presence of 20 μM PIP_2 and 100 μM Ca^{2+} it takes at least 2.5 minutes longer for the current to become undetectable when compared to ano1 in the presence of only 100 μM Ca^{2+}. A likely binding site for PIP_2 was found on TM 3-5 which matches up with the results of Yu et al. (2019). The Ca^{2+} binding site was found on TM 6-8. The PIP_2 binding site was identified

by a mutagenesis screening conducted in HEK293 cells that elucidated six key basic amino acids in PIP_2 binding.

Mutagenesis was utilized by Le et al. (2019) and two locations for basic residues identified to impact PIP_2 binding were the same as those identified by Yu et al. (2019). This data indicates a possible location for PIP_2. However, Le et al. (2019) state that at these locations in the amino acid sequence lysine was being replaced while Yu et al. (2019) state that it is arginine being replaced. Both studies were examining mouse ano1 structure which would imply the same amino acids should be in the same location for both studies. However, they used sequences from different databases to run the MD simulations. Though the amino acids were different they are both basic residues so it may not have a significant impact on the results of simulations.

Peters et al. (2018) determined that the conformation of ano1 depends on Ca^{2+} binding and voltage changes via MD simulations and patch-clamp electrophysiology experiments using mouse Ano1. TM 6 is a flexible helix and likely has a hinge point at the 640^{th} amino acid, which is a glycine (Peters et al., 2018). When a single Ca^{2+} ion binds, ano1 has a conformational change in TM 6 allowing some Cl^- to exit the cell (Figure 5B). Once two Ca^{2+} ions bind to the channel it fully opens (Figure 5). When PIP_2 binds to ano1 it stabilizes the open conformation and attenuates the desensitization that occurs when just Ca^{2+} is bound. When only PIP_2 or a single Ca^{2+} is bound to ano1 it is partially open. Long-chain PIP_2 had a more sustained impact on the current when compared to diC_8 PIP_2 (Le et al., 2019).

The studies conducted by Yu et al. (2019) and Le et al. (2019) that used diC_8 PIP_2 could have produced results that differed from those that used full-length PIP_2. diC_8 PIP_2 is a

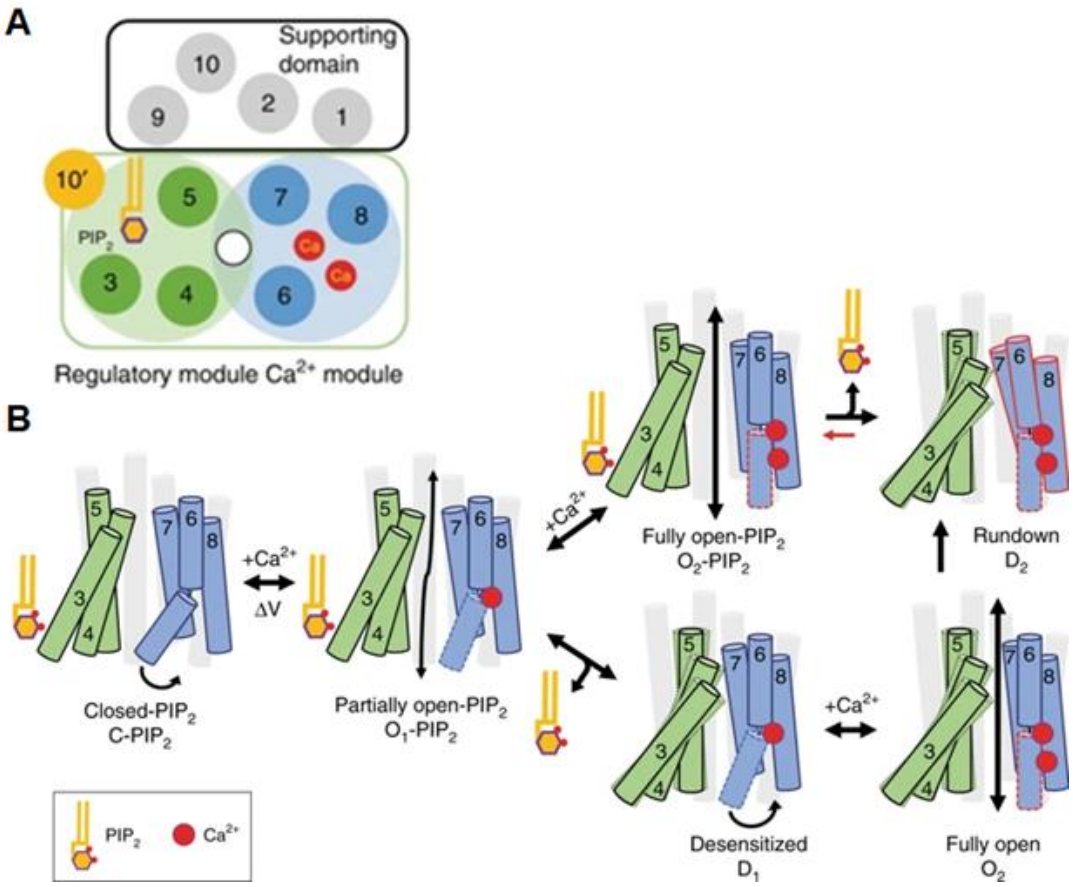

Figure 5. Ano1 conformation with Ca^{2+} and PIP_2 bound. A) Cross sectional view of Ano1 with PIP_2 and 2 Ca^{2+} bound B) Proposed model for the conformational changes with different modulatory proteins bound. TM 6 is proposed to hinge open when 2 Ca^{2+} ions bind. PIP_2 binding prevents Ca^{2+} desensitization allowing Ano1 to remain open longer (Le et al., 2019).

water-soluble short acyl chain PIP_2. Due to the shorter acyl chain on diC_8 PIP_2, it is more likely to be washed off of the membrane resulting in a more transient impact (Le et al. 2019). When PIP_2 is bound to ano1 its acyl tail sits in a cavity of the dimer which helps stabilize its interactions. When the tail is shortened, the interaction becomes less stable. To understand the interaction more accurately between PIP_2 and ano1 *in vivo* I think that only full-length PIP_2 should be utilized for experiments.

Ano1 function in intestinal ICC

For the GI tract to efficiently digest food and absorb essential nutrients, coordination of the iSM contractions in the intestinal wall is necessary (Singh et al., 2014). Electrical slow waves that move through the ICC network control proper iSM contraction. Zhu et al. (2009) were the first to provide evidence that the Ca^{2+}-activated Cl^- current (CaCC) was likely a result of ano1 function and controlled slow wave activity. They showed that Cl^- permeability was abolished in the absence of Ca^{2+} which also indicated that ano1 was likely controlling the current being observed. The rate of energy transfer of the current produced by ano1 is 8 pS in HEK293 cells and Zhu et al. 2009 determine the CaCC in ICC from the small intestines of mice was 7.8 pS which is a good indication that they were looking at the current controlled by ano1 (Yang et al., 2008). When this current was blocked by niflumic acid (a chloride channel blocker), a concentration-dependent decrease in slow waves was observed. This provided more evidence that ano1 was controlling the slow wave.

Through experiments on the isolated small intestines of mice, ano1 was determined to be necessary for the proper function of ICC (Hwang et al., 2009; Singh et al., 2014). Hwang et al. (2009) removed the small intestine from ano1 knockout (KO) mice at postnatal day 0 and cultured it for 6-7 days. They found a complete loss of slow wave activity in the ano1 knockout mice (Hwang et al., 2009). By contrast, $ano1^{+/-}$ mice had no difference in activity compared to $ano1^{+/+}$ indicating that only one copy of ano1 is required for proper function (Hwang et al., 2009). Similar results were found by Sing et al. (2014). For these experiments, small intestines from ano1 KO mice were maintained in an organ bath. Consistent with the previous studies, slow electrical waves were absent. iSM contractions were non-rhythmic and had lower amplitude (or force). In wild-type mice, spontaneous and coordinated Ca^{2+} transien

was observed, and in ano1 knockout (KO) mice spontaneous and uncoordinated Ca^{2+} transients was observed (Singh et al., 2014). The function of ano1 is to control the slow wave by coordinating Ca^{2+} transients. Therefore, it makes sense that when ano1 is knocked out, Ca^{2+} transients is impacted. However, in the presence of nicardipine, an L-type Ca^{2+} channel blocker, slow waves persisted even though L-type Ca^{2+} channels are known to be present on ICC (Drumm et al., 2017). When T-type Ca^{2+} channel blockers were added, a significant decrease in slow waves was observed (Drumm et al., 2017). These results indicate the T-type Ca^{2+} channels are necessary for proper slow wave propagation (Drumm et al., 2017)

Function of Ano1 in the SIP syncytium

The SIP syncytium is hypothesized to be a functional unit that controls coordinated slow waves and iSM contractions (Sanders et al., 2014). It is proposed that signals from the enteric nervous system are sent to the ICC and PDGFRα+ cells via synapses. The signal is then relayed to the iSM via gap junctions. The PDGFRα+ cells are fibroblast-like cells that are poorly-understood (Iino et al., 2009). In 2011, PDGFRα+ cells were found to have a role in relaying signaling from inhibitory neurotransmitters to iSM (Kurahashi et al., 2011). Currently, ICCs are the main cellular network being studied to elucidate how proper intestinal function is controlled.

As mentioned earlier, there are receptors that bind the neurotransmitter acetylcholine which can activate the pathways that activate ano1. Ca^{2+} release from the ER is triggered downstream of M_3 muscarinic receptors being bound by an agonist. This Ca^{2+} release from the ER is required for activation of ano1. When ano1 is inhibited, electrical slow wave activity decreases or ceases completely. Drumm et al. (2019) proposed that inhibition of slow

waves may be due to nitrergic inhibition acting indirectly on ICC by preventing Ca^{2+} release events from occurring, therefore, preventing the activation of ano1. Nitrergic inhibition is the inhibition of activity that is triggered by neurons that release nitric oxide (NO). Baker et al. (2018) investigated nitrergic signaling in ICC of the mouse small intestine. Using fluorescently-activated cell sorting, they found that there were five downstream mediators of nitrergic signaling that had higher expression in ICC when compared to all of the intestinal cells examined (Baker et al., 2018). Because ICCs mediate signaling between the ENS and the iSM, it has been hypothesized that NO acts indirectly on ICC (Drumm et al., 2019b). To investigate how nitrergic inhibition impacts the slow wave, tetrodotoxin (TTX, a nerve blocker) or L-NNA (an inhibitor of NO synthesis) was added to an intact, excised mouse colons (Drumm et al., 2019b). Muscle contraction frequency and amplitude increased with the addition of either of these molecules, indicating the NO has an inhibitory effect on ICCs (Drumm et al., 2019b). This effect was canceled out by the addition of ano1 antagonists showing that the downstream effect of NO is inhibition of ano1 activity. Though this pathway inhibits ano1, no direct evidence was provided to show that NO acts directly on ICC since they are electrically coupled to the other cells in the SIP syncytium.

The way in which PDGFRα^{+} cells receive and relay signals in the SIP syncytium needs to be determined since it is likely that these cells were still present in the tissue samples being tested. Since these cells are electrically coupled with ICC, it is possible that the PDGFRα+ cells receive inhibitory input and relay that signal to the rest of the SIP syncytium which leads to all the downstream results recorded in the ICC. It is also possible that combined signaling from both ICC and PDGFRα+ is necessary for inhibition. While the investigators had the necessary specific controls to compare against the neuron-ICC

interactions, they did not have controls for the potential contribution of PDGFRα+ cells. Currently, there is no evidence showing that PDGFRα+ cells have a role in nitrergic inhibition, slow wave propagation, or iSM contraction.

While PDGFRα+ cells have not been shown to have a role in relaying signals from nitrergic inhibition, they have been shown to have a role in relaying signals from purinergic inhibition. Purinergic inhibition is the inhibition of activity by purines such as adenosine. Purinergic receptors expressed on PDGFRα+ cells appear to have no impact on the Ca^{2+} transiency in ICC. The impact of purinergic regulation on ano1 function remains unresolved, but it may not have a role in regulating ano1 since its activation or inhibition did not impact Ca^{2+} transiency in ICC.

Activation of the G-protein coupled pathway (GPCR) could be the mechanism for autorhythmicity in ICC. When the GPCR is activated, this leads to the production of the substrate IP_3 via hydrolysis of PIP_2 by PLC, which is necessary for Ca^{2+} release via IP_3R1 channels on the ER to occur. It has been shown that acetylcholine transmits excitatory signals to ICC via M_3 receptors (Wang et al., 2003). These experiments were conducted by placing the small intestines from mice in organ baths (Wang et al., 2003). The addition of the M_3 receptor agonists carbachol and acetylcholine increased the frequency of slow waves in both intact intestinal muscle and cultured ICC from mice (Kim et al., 2003). As with intrinsic slow waves, the signal would then get relayed from the ICC to the iSM.

Ano1 function on other cell membranes vs. ICC membrane

Other cells that express ano1 include the smooth muscle cells and epithelial cells within the airways, and smooth muscle cells in arteries (Bao et al., 2008; Bulley et al., 2012).

The function of ano1 in different cell types varies. On the plasma membrane of both ICC and smooth muscle in the airway and arteries, ano1 activation is tightly coupled with Ca^{2+} release from the ER (Jin et al., 2016). In ICC, the main Ca^{2+} release channel on the ER is IP_3R1 whereas in airway smooth muscle it is the ryanodine receptors (RyRs) (Bao et al., 2008). In the ICC, ano1 is activated by Ca^{2+} release from the ER and may be supplied with Ca^{2+} by voltage-dependent Ca^{2+} channels (VDCC) after Ca^{2+} release from the ER begins. By contrast, in cerebral artery smooth muscle, ano1 activation is coupled to Ca^{2+} influx through non-selective stretch-activated cation channels on the cell membrane (Bulley et al., 2012).

IP_3R1, IP_3R2, and IP_3R3 are all expressed on smooth muscle cells that line the airway (Wang et al., 2004). Although these receptors are expressed on these smooth muscle cells, they have not been shown to be in close proximity to the ano1 channels that are expressed. However, it is hypothesized that, within ICC, IP_3R1 channels are in close proximity to ano1 since the IP_3R1 channel is proposed as the initial activation mechanism for ano1 (Ward et al., 2000). Ano1 activity in smooth muscle, in general, is mediated by the agonistic neurotransmitters noradrenaline, histamine, and endothelin via the upregulation of intracellular Ca^{2+} release (Jin et al., 2016). Consistent with this, ano1 activity on airway smooth muscle is increased by the addition of the synthetic nonselective muscarinic receptor agonist methacholine (Huang et al., 2012). As in ICC, this is a G-protein coupled pathway that ultimately leads to smooth muscle contraction by activation of ano1 (Huang et al., 2012). This pathway has been identified as a potential target for treating asthma by applying antagonists to reduce the frequency of muscle contraction (Danielsson et al., 2015).

Ano1 on epithelial cells lining the lumen of the GI tract and the respiratory tract has been shown to modulate mucous secretion, unlike ano1 on ICC (Huang et al., 2012).

Overproduction of mucous secretion is a feature of asthma, which further strengthens ano1 as a target for treating asthma (Huang et al., 2012). Though the function of ano1 differs from cell type to cell type, it is becoming obvious that this CaCC has a lot of potential as a target in treating different diseases.

Trpa1 channels in the GI tract

TRPA1 channels are present in the GI tract of humans (Prober et al., 2008). There are two paralogs of TRPA1 in zebrafish, *trpa1a* and *trpa1b* (Prober et al., 2008). While this gene is expressed in zebrafish it has only been studied in the head of zebrafish. It is important that the expression patterns of these genes within the GI tract be determined for zebrafish. In mammals, TRPA1 is known to increase intestinal motility in the presence of stimuli like trans-cinnamaldehyde (Bellono et al., 2017). Since trans-cinnamaldehyde can be an irritant at certain concentrations, the increase in intestinal motility occurs in order to protect the mucus lining of the intestines (Bellono et al., 2017). It would be interesting to determine if there is a concentration of trans-cinnamaldehyde that can increase intestinal motility without irritating the GI tract. Zebrafish provide a useful model system to set up an experiment that could test out this hypothesis.

Objectives of This Study

The purpose of this study was to gain a better understanding of how intestinal motility is controlled. I had two main objectives: first, to develop an intestinal motility model and second, to investigate how sensory receptors may influence ICC activity. I developed an intestinal transit assay using zebrafish so that I could observe intestinal motility. To better

understand ICC activity, I focused on stretch receptors and the Trpa1a nutrient receptor. I demonstrated that activation of stretch receptors alone was not sufficient to simulate normal intestinal motility. I also demonstrated that stimulating Trpa1a channels with the agonist trans-cinnamaldehyde (TC) increases intestinal motility.

Materials and Methods

Husbandry

Zebrafish were approved for use by the Institutional Animal Care and Use Committee at Appalachian State University (IACUC #19-02). Animals were all wild type, obtained from a local pet shop. Adults were raised according to *The Zebrafish Book: A Guide for the Laboratory Use of Zebrafish Danio (Brachydanio rerio)* (Westerfield, 2007). Water quality was tested daily so the temperature was maintained at 27ºC to 28ºC, the pH was between 6.8-7.2, and the conductivity was between 600-850 microsiemens. Fish were fed dry food at 9:00AM and 48-hour old brine shrimp (*Artemia franciscana*) at 3PM. The zebrafish were kept on a 14-hour light cycle from 9:00AM to 11:00PM.

Larvae were obtained by crossing adults from the Kinkel/Bouldin Lab in the Zebrafish Core Facility. Eggs and larvae were raised following the guidelines from Norton et al. (2018). Once laid, eggs were transferred to a fishbowl with ~120 mL of E3 medium (5 mM NaCl, 0.17 mM KCl, 0.33 mM $CaCl_2$, 0.33 mM $MgSO_4$) with the addition of 0.01% methylene blue. On the day the eggs were collected they were bleached and thoroughly rinsed with facility water. Once bleached, the eggs were sorted so that there were 50 eggs per culture bowl. The bowls were placed in an incubator at 28.5ºC until 5 dpf. On 3 dpf, the embryos were manually dechorionated. On 5 dpf, the larvae were transferred to nursery tanks with ~250 mL of E3 and were kept at ~28.5ºC. From 5-9 dpf, the larvae were fed dry food suspended in E3 at 9:00AM and 3:00PM and 24-hour old brine shrimp at 12:00PM. The dry food was Golden Pearl (GP) Reef and Larval Diet (Brine Shrimp Direct). The food mix was equal amounts of GP5-50 microns and GP50-100 microns suspended in E3 and stored at 4ºC. Brine shrimp were cultured at 12:00PM in a shrimp hatchery filled with ~725 mL of 30 g/L

Instant Ocean salt dissolved in deionized reverse osmosis water. The hatchery was kept at ~26.5ºC.

Intestinal Transit Assay—Basic Protocol

Larvae were acquired and raised following the guidelines previously stated until 3:00PM on 8 dpf. On 8 dpf, larvae were fasted overnight. To fast, larval tanks were changed prior to the 3:00PM feeding and then fed as usual. At ~5:00PM tanks were thoroughly cleaned using a wide-bore fire blasted pasture pipette to remove loose debris. Each tank was filled with fresh E3 and siphoned down to ~250 mL 2-3 times to remove any remaining debris. Tank lids and tanks were labeled "fasted".

The following morning, 9 dpf larvae were fed 24-hour old brine shrimp at 9:00AM. After feeding for 15 minutes, tanks were siphoned down so that the remained contents would fit into a 100 mm Petri dish. Larvae were anesthetized with 0.4% tricaine and screened under an Olympus SZX12 microscope or a Leica MDG41 microscope to sort for larvae that had consumed a brine shrimp. A fish line probe was used to position the larvae lateral for better view of the intestinal bulb. Larvae that had eaten a shrimp were placed in a fresh tank of E3 medium for recovery from anesthesia and were returned to the nursery. The new tank was kept on a heating block to maintain 28.5ºC unless otherwise stated. At specific time-points after feeding, intestinal contents were imaged through the body wall of live larvae to track gut transit.

Intestinal Transit Assay—Detection of Decreased Intestinal Motility

The basic protocol described above was followed until after the larvae were sorted. During the sorting process the experimental tank was kept on the countertop to maintain room temperature E3. Once sorted, the experimental tanks were placed in a room temperature water bath (~20ºC) while the control tanks were placed back into the nursery set to 28.5ºC. Images were tank 3, 4, 6, and 7 hours after feeding began. A new tank was used for each timepoint so now larvae were imaged twice.

Intestinal Transit Assay— Detection of Increased Intestinal Motility with Brine Shrimp

The larvae were raised following the basic protocol until the sorting process. Prior to beginning the sorting process recovery tanks were set up with 250 mL of E3 medium. The larvae with shrimp in the intestinal bulbs were placed in the recovery tank. The tanks were placed back into the 28.5ºC tabletop nursery. Experimental tanks were given 1.57 µL TC (Sigma Aldrich, W228613) for a final concentration of 0.05 mM. For control tanks, 1.57 µL of E3 medium was pipetted into the tank. Fish were imaged on both an Olympus SZX12 microscope and a Leica MDG41 microscope at 2, 3, 4, and 5 hours after treatment.

Intestinal Transit Assay—Detection of Increased Intestinal Motility with Nile Red

The larvae were raised following the basic protocol until 5 pm on 8 dpf. At 5 pm on 8 dpf tanks were siphoned down and fish were poured into a 100 mm Petri dish to be anesthetized with 10-20 drops of 0.4% tricaine. The fish were then sorted into small fishbowls containing 4.95 mL of E3 medium and 0.05 mL of 100X Nile Red (Sigma Aldrich, N3013) in acetone stock solution (1,000 µg Nile Red/L acetone) to give a final concentration of 10µg/L. The Nile Red stock solution was kept in the dark at 4ºC. Each bowl contained 5

larvae per 5 mL E3. The bowls were placed in an incubator set to 28.5ºC overnight. The next morning at 9 am, each bowl of fish was washed 3 times with E3 medium to remove excess Nile Red. To wash the Nile Red off, 40-micron cell strainers were used to move the larvae from one bowl of E3 to the next bowl of E3. After washing, the bowls were weighed and E3 was either added or taken out until the weight of the E3 was 5 g. This was done to ensure that the final concentration was consistent from bowl to bowl. The bowls were then treated with either 0.025 mM TC, 0.05 mM TC, or >1% DMSO in 0.5X E3 medium. The fish were processed for imaging as described below. The TC solutions were diluted in E3 medium with 10% DMSO. The final concentration of DMSO was <1%. Imaging was conducted 6 and 24 hours after treatment.

Live Imaging

For live imaging with brine shrimp as the contents of the intestinal bulb, the larval tanks were siphoned down so that the remaining E3 medium could be poured into a 100 mm Petri dish. The zebrafish were anesthetized using 10-20 drops of 0.04% M tricaine added drop wise with a Pasteur pipette. For live imaging with Nile Red as the contents of the intestinal bulb, 3-5 drops of 0.04% tricaine was added drop wise with a Pasteur pipette. Once anesthetized, larvae were transferred on to a 3% agarose gel mold (World Precision Instruments) using a wide-bore fire-polished Pasteur pipette. The mold had small lanes in it to help orient the fish laterally. The larvae stayed submerged in E3 medium during imaging. A fish line probe was used to orient the larvae laterally. Temperature was maintained using prewarmed 28.5 ºC E3 medium and a heat block or by maintaining the dish on the bench at room temperature (~20.0 ºC). A Canon EOS Rebel T5i camera attached to an Olympus

SZX12 microscope and a Canon EOS Rebel T5i attached to a Leica MDG41 microscope were used to capture the images. For fluorescent imaging with Nile Red, a green light and filter set with an excitation range of 510-540 nm and emission of 600nm was used (NIGHTSEA).

Intestinal Dissection

Intestines were dissection from wildtype adult zebrafish following the guidelines published by Eames-Nalle et al. (2017). Briefly, fish were euthanized with cryoanesthesia followed by decapitation with CeramaCut® Scissors (Fine Science Tools). Specimen were pinned semi-laterally to a dissection dish and a cut was made using Vannas spring scissors (World Pression Instruments, 501777) along the ventral midline past the pelvic girdle. A two perpendicular cuts were made at the caudal end of the incision into the axial muscle. The flaps were open using forceps (Fine Science Tools, 11270-20) and the organs were removed from the body cavity. The specimen remained submerged in E3 medium throughout the dissection process. All organs, including the heart, gonads, liver, and swim bladder, were removed to fully isolate the intestines. The intestine was cut into 3 segments: the intestinal bulb (IB), the proximal region of the intestinal loop, and the distal small intestine and colon.

RT-PCR primers

The *ada, apq4,* and *slc10a2* primers were designed using Primer-BLAST (Ye et al., 2012) and were used as controls (Table 3). Expression of *ada* is specific to the IB, expression of *slc10a2* is specific to the small intestine, and expression of *apq4* is specific to the posterior intestine (Lickwar et al., 2017; Tingaud-Sequeira et al., 2010). The *ano1* primers were from

Jiang et al., (2018), the *kita* primers were from Rich et al., (2007), the *trpa1a* primers were from Corey et al. (2004) and the *trpa1b* primers were from Prober et al. (2008) (Table 3). The primers were confirmed using Primer-BLAST.

Table 3. RT-PCR primer sequences for spatiotemporal mapping of expression throughout the gastrointestinal tract of zebrafish.

Name	Sequence	Expected size (bp)
ada	F: 5'-ATTGGGCACGGATACCACA-3' R: 5'-GCATGCCGTAGGCCTCATA-3'	161
aqp4	F: 5'-AGTCTGAGGAGGAATGACAAGC-3' R: 5'-GTTGCGATGGACAAGCCAAA-3'	267
slc10a2	F: 5'-ATCTGTGGTGGGAATCGTCC-3' R: 5'-GCGTTCTGCATGCCTGTTTC-3'	143
ano1	F:5'-CGAGAGCGGAGTATGAGTTTC-3' R: 5'-GGTCATGTAAGCTGGCATTCT-3'	116
kita	F: 5'- GTTATCCCACTCCTCAGATCAAGT -3' R: 5'- TCACAGCTACAGTCATCACAGTGT -3'	564
trpa1a	F: 5'-CAGGTGGCTTCAGCATCCA-3' R: 5'-GGTTAGCTCTCGTTCCAGTG-3'	1150
trpa1b	F: 5'-CTTTTGCTGGCTTTCGGCTT-3' R: 5'-TGTTCTTCTGCTTGTGCAGC-3'	514

Statistical analysis

ImageJ software was used to determine the fluorescence intensity of Nile red within the intestinal bulb. The region of interest (ROI) was selected by hand. Microsoft Excel was used to conduct student t-tests.

Results

Cooling tank temperature results in slower transit.

In order to study intestinal function, a reliable intestinal transit assay that could distinguish between a normal and altered intestinal transit time needed to be developed. Since fish are poikilotherms whose metabolism rate is largely controlled by the external temperature, a decrease in tank water temperature was used as a treatment. First, an effective method for cooling the tanks to room temperature was needed. I asked whether transferring tanks from the 28.5ºC nursery to a room temperature nursery would cool the tank water rapidly enough to decrease the temperature during the digestion phase. To test this, a tabletop nursery at room temperature was set up alongside the 28.5ºC tabletop nursery. Three tanks with 250 mL of E3 medium and no fish were warmed to 28.5ºC in the nursery. Once the tanks reached 28.5ºC they were transferred to the room temperature nursery. The time it took for the tank medium to reach room temperature was recorded. It was determined that it took approximately 50 minutes for the water temperature to drop to room temperature (~20.0ºC) (Figure 6). As shown in Figure 6, the tank water dropped by 2.5ºC within 5 minutes of the transfer and 4.5ºC within 10 minutes. This relatively rapid decrease in temperature was predicted to slow metabolism and therefore slow intestinal transit.

Once an efficient method for cooling the tanks was developed, an intestinal transit assay comparing the transit time in larvae kept at room temperature (~20.0ºC) to larvae kept at 28.5ºC was developed. However, a pilot study with 7 dpf larvae revealed that no larvae would consume brine shrimp while at cool temperatures. Therefore, all subsequent experiments allowed the zebrafish to feed for 15 minutes at their preferred temperature of 28.5ºC before transferring the tanks to the cool nursery.

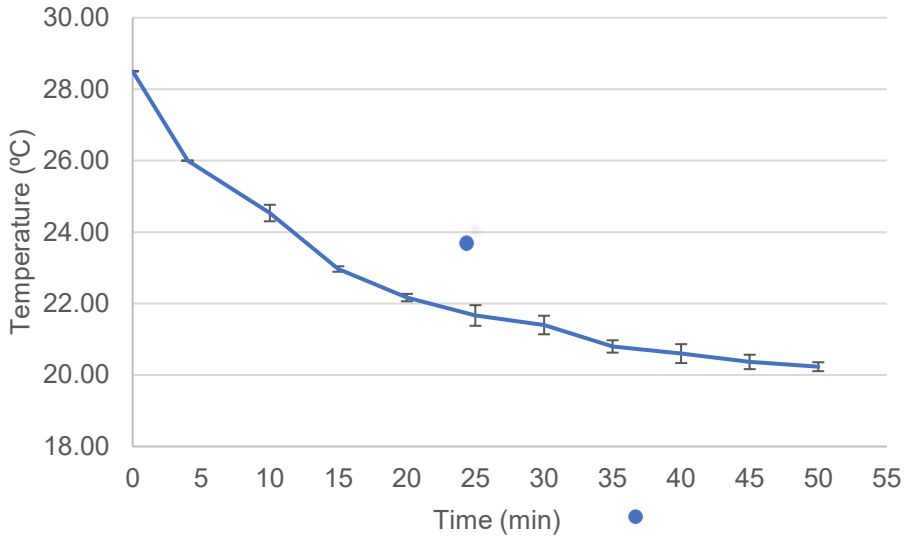

Figure 6. The average time required for a tank at 28.5ºC to reach room temperature (~20.0ºC). The data shown are the averages of three tanks per time point. Error bars indicate standard deviation.

With the revised protocol, another pilot study was conducted on 7 dpf. For this study, larval zebrafish were fasted overnight then fed brine shrimp at 9:00 AM the next morning and allowed 15 minutes to feed at 28.5°C. Larvae were then anesthetized and sorted for those that had consumed a brine shrimp. After 15 minutes of feeding, the experimental tanks were moved to the room temperature tabletop nursery. This study was conducted to determine the most efficient way to conduct imaging and the timepoints for imaging (Figure 7). This revealed that the control larvae appeared to empty their intestinal bulbs around 4 hours after feeding when kept at 28.5ºC (Figure 7A), which is consistent with previous work. The larvae kept at room temperature still had chyme and grey debris remaining in the intestinal bulb 4 hours after being fed. This showed that cooler temperatures lead to slower intestinal transit. To determine how long it takes for the larvae at room temperature to fully digest the brine shrimp another study was conducted but with the timepoints extended out to seven hours after being fed.

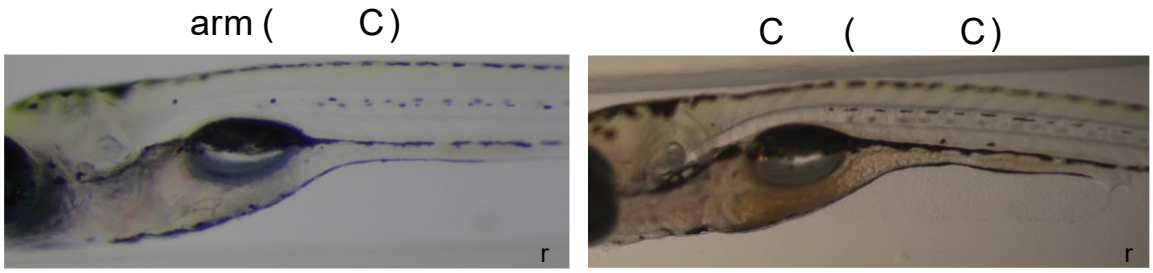

Figure 7. Imaging pilot study with 7 dpf zebrafish to test the impact of a cooler water temperature on intestinal transit rate. The larvae kept in the warm water bath (A) had an empty intestinal bulb 4 hours after feeding (n=1) while the larvae kept in the cold water bath (B) still had brine shrimp present in the intestinal bulb (n=3). Live images. All larval heads are to the left of the images

Intestinal transit assay experiments with extended timepoints were conducted using nine dpf larvae because a previous study in the Kinkel lab showed that approximately 60% of larvae consumed a brine shrimp by this day of development. By contrast, only 20% of seven dpf larvae consume a brine shrimp. The same protocol that was used for the pilot study was followed here except that the larvae were fasted starting on eight dpf and imaged on nine dpf. On nine dpf, imaging began three hours after feeding brine shrimp to the larvae. For the larvae kept at 28.5ºC, the intestinal bulb had gray debris remaining three hours after being fed (Figure 8A). By four hours after feeding, the intestinal bulb was empty (Figure 8B). By contrast, the larvae kept at room temperature still had brine shrimp left in the intestinal bulb three and four hours after being fed (Figure 8C, D), consistent with the results using seven dpf larvae. By six hours there was a small amount of gray debris remaining in the intestinal bulb for the larvae kept at room temperature (Figure 8E). Seven hours after being fed the intestinal bulb was empty (Figure 8F). These results show that cooled temperatures result in slowed intestinal transit, as predicted, and that imaging the intestinal contents of live larvae is feasible. These results also show that this intestinal transit assay can detect a difference between normal and altered intestinal transit time.

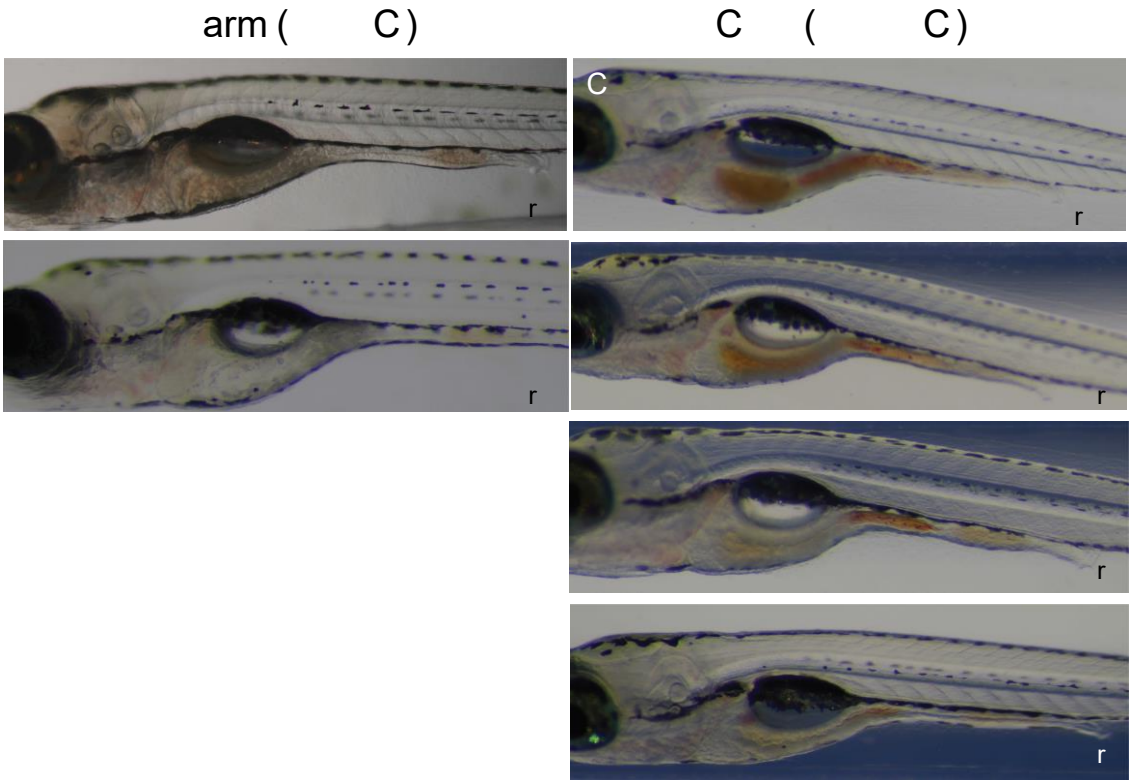

Figure 8. A decrease in water temperature leads to a decrease in intestinal transit rate. The warm group was kept at 28.5ºC during digestion while the cold group was transferred to ~20.0ºC during digestion. A) Three hours after being fed, some brine shrimp was present in the intestinal bulb (the darker color in the intestinal bulb), n=26. B) Four hours after being fed, the intestinal bulb was empty (n=13). C) Three hours after being fed, the intestinal bulb was full with brine shrimp (n=13). D) Four hours after being fed, of brine shrimp was still present in the intestinal bulb (n=29). E) Six hours after being fed, the intestinal bulb was mostly empty, with some traces of chyme remaining (n=29). F) Seven hours after being fed, the intestinal bulb was empty (n=32). Live images at 9 dpf. All larval heads are to the left of the images

Cinnamaldehyde causes an increase in intestinal transit rate

To activate the nutrient receptor trpa1a in the intestinal epithelium, the Trpa1-specific ligand TC was used. This agonist is known to stimulate gut motility in mammals (Bellono et al., 2017). To determine if there was a concentration of TC that is sufficient to stimulate gut motility in zebrafish, three concentrations of TC were tested. Larval zebrafish were fasted overnight on eight dpf. They were fed brine shrimp at 9:00 AM the next morning and allowed 15 minutes to feed. Larvae were then anesthetized and sorted for those that had consumed a brine shrimp. The larvae were then treated with 0.05 mM, 0.025 mM, or 0.005

mM TC. Controls were given E3 medium. As expected, the controls had largely completed digestion within four hours of feeding. As shown in Figure 9A, A', the intestinal bulbs showed a small amount of chyme remaining, and some gray debris was visible in the posterior intestinal bulb. By contrast, the group treated with 0.005 mM TC showed faster intestinal transit. Figure 9B, B' shows that within three hours after being fed, TC-treated larvae had no visible chyme in their intestinal bulbs. Some gray debris is visible in the posterior intestinal bulb. The group treated with 0.025 mM TC showed similar results (Figure 9C, C'). However, the group treated with 0.05 mM TC had a completely empty intestinal bulb within 3 hours after being fed (Figure 9D, D'). This suggests that, like mammals, zebrafish have Trpa1 receptors in their intestinal epithelium.

In order to get a larger sample size and for more timepoints another experiment was conducted. Since the larval treated with 0.05 mM TC had empty intestinal bulbs after 3 hours, this concentration was used for the next set of experiments. After the larvae were sorted for brine shrimp in the intestinal bulb, they were treated with 0.05 mM TC. Images were taken two, three, four, and five hours after being treated. As observed in previous experiments majority of the larval zebrafish from the control group had an empty intestinal bulb four hours after being fed (Figure 10, Table 4). Majority of larvae treated with 0.05 mM TC, had empty intestinal bulbs three hours after being treated (Figure 10, Table 4). This indicates the TC increases the intestinal motility in zebrafish.

Nile red can be utilized to observe intestinal transit in the absence of nutrients

To allow for targeting the Trpa1 receptors, the non-nutritive tracer Nile red was used to fill the intestinal bulb prior to TC treatment. The rationale was to observe the effects of

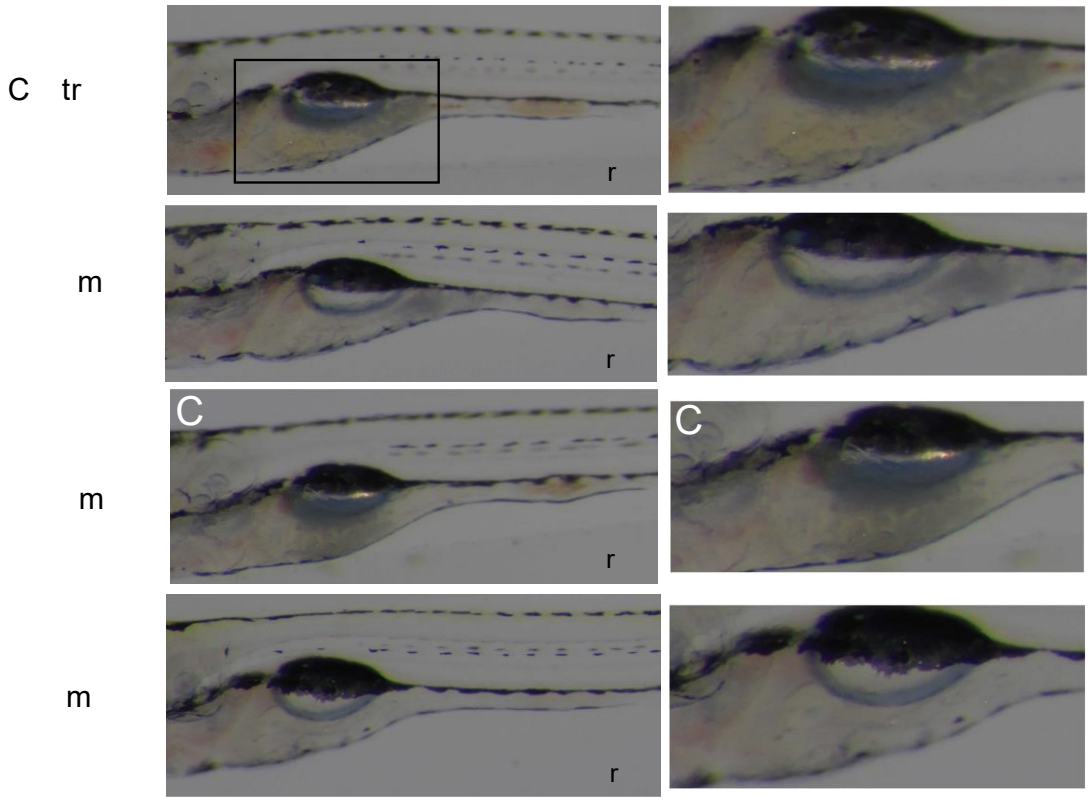

Figure 9. Transcinnamaldehyde (TC) concentration pilot study using 9 dpf zebrafish. (A, A') Four hours after feeding, the control group had some chyme (pale orange/yellow color) remaining in the anterior intestinal bulb and some gray debris in the posterior intestinal bulb (n=14). (B, B') Three hours after feeding, the group treated with 0.005 mM TC had empty intestinal bulbs except for some gray debris remaining distally (n=24). (C, C') The group treated with 0.025 mM TC similarly had empty intestinal bulbs except for gray debris remaining in the intestinal bulb (n=17). (D. D') The group treated with 0.05 mM TC had an empty intestinal bulb. The box in panel A indicates the region of interest for panels A'-D'. Larvae imaged live, with heads shown to the left in all panels.

TC on the distended intestinal bulb in the absence of any other nutrients. Before conducting these experiments, the concentration of Nile red needed to fill the intestinal bulb was determined. Small fishbowls were set up with either 0.0314 μM or 0.314 μM Nile red. The larvae were incubated in the Nile red for 16 hours and were then washed. Images were taken 30 minutes, four hours, and six hours after the wash. As shown in Figure 11, both concentrations yielded similar results and, in both cases, the Nile red was easily observable through the body wall. For both treatment groups, the intestinal tracts remained filled with Nile red for at least six hours after washing off the treatment. The 0.0314 μM Nile red concentration was determined to be sufficient for filling the intestinal bulb.

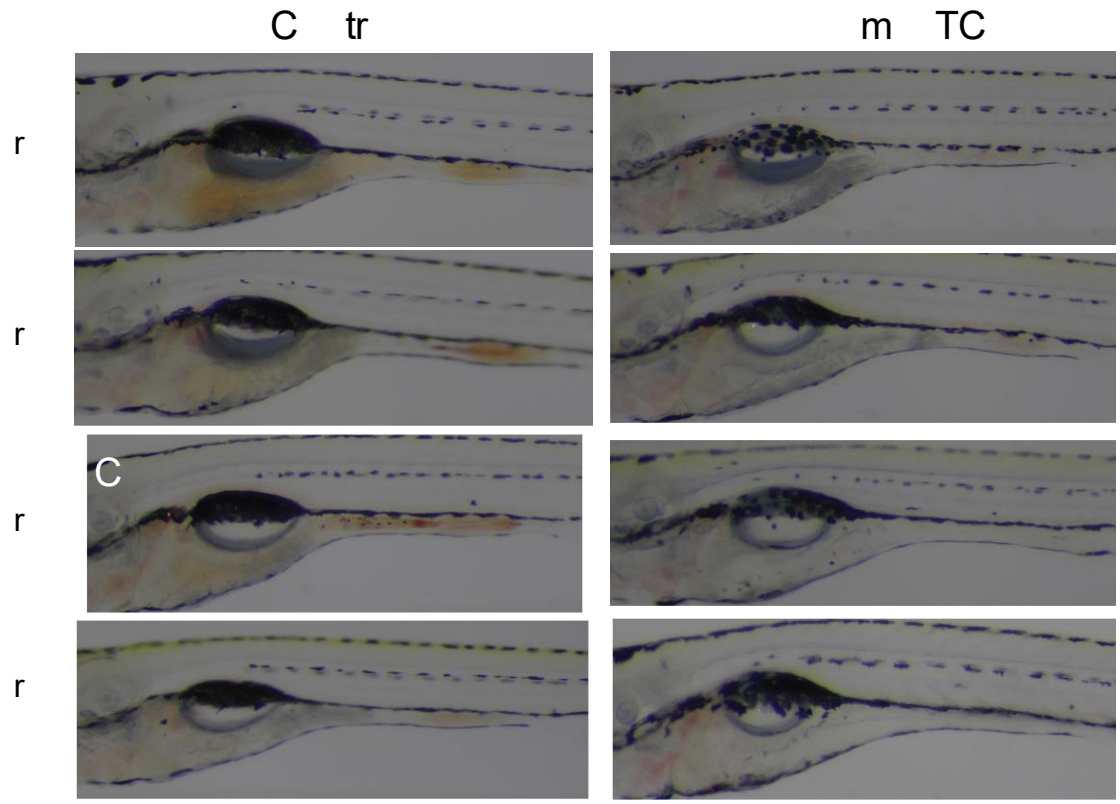

Figure 10. Treatment with TC causes an increase in intestinal transit rate. On 9 dpf larvae were fed brine shrimp and treated with E3 medium (control) or 0.05 mM TC 15 minutes later. For the control group A) two hours after feeding there was chyme left in the intestinal bulb (orange) (n=22) B) three hours after feeding there was gray debris remaining in the intestinal bulb with some chyme in the mid-intestine (n=21) C) four hours after feeding the intestinal bulb was mostly empty with some gray debris (n=12), and D) five hours after being treated the intestinal bulb was empty. For the group treated with 0.05 mM TC E) two hours after feeding there was some gray debris remaining in the distal part of the intestinal bulb (n=20) F-H) three, four, and five hours after feeding the intestine bulb was empty (n=17 for 3 hours; n=17 for 4 hours; n=15 for 5 hours). All larval heads are to the left of the images

Table 4. The impact TC treatment has on intestinal transit rate of 9 dpf larval zebrafish. The timepoints are referring to the amount of time that passed after treatment with TC.

	Chyme (%)		**Debris (%)**		**Empty (%)**	
	Control	**Treated**	**Control**	**Treated**	**Control**	**Treated**
2-hour	95.5	7.2	4.5	21.4	0	71.4
3-hour	57.1	0	42.9	50.0	0	50
4-hour	50.0	11.0	16.7	23.5	33.3	64.7
5-hour	31.25	0	31.25	40.0	37.5	60.0

In addition to providing a strong signal for observing intestinal transit, Nile red treatment also allows for imaging the contractions of the intestinal wall that occur in response to stretch-sensitive receptors. As shown in the time series in Figure 12, distinct points of constriction of the intestinal lumen can be observed.

Next, a pilot study was conducted to test whether TC treatment would elicit an increased transit rate in the absence of other nutrients. To fill the intestinal bulb, fasted larvae were incubated in Nile red for 16 hours starting at 5 PM on 8 dpf. After being washed on 7 dpf, the larvae were treated with either 0.05 mM TC or 0.025 mM TC and imaged six hours and 24 hours after being treated. As shown in Figure 13, there was a significant difference in the intensity of Nile red in the intestinal bulb six hours after treatment (control versus 0.05 mM TC, $p < 0.0005$, control versus 0.025 mM TC, $p < 0.005$). At six hours after treatment, there was no significant difference in fluorescence intensity for larvae treated with either concentration of TC ($p = 0.482$).

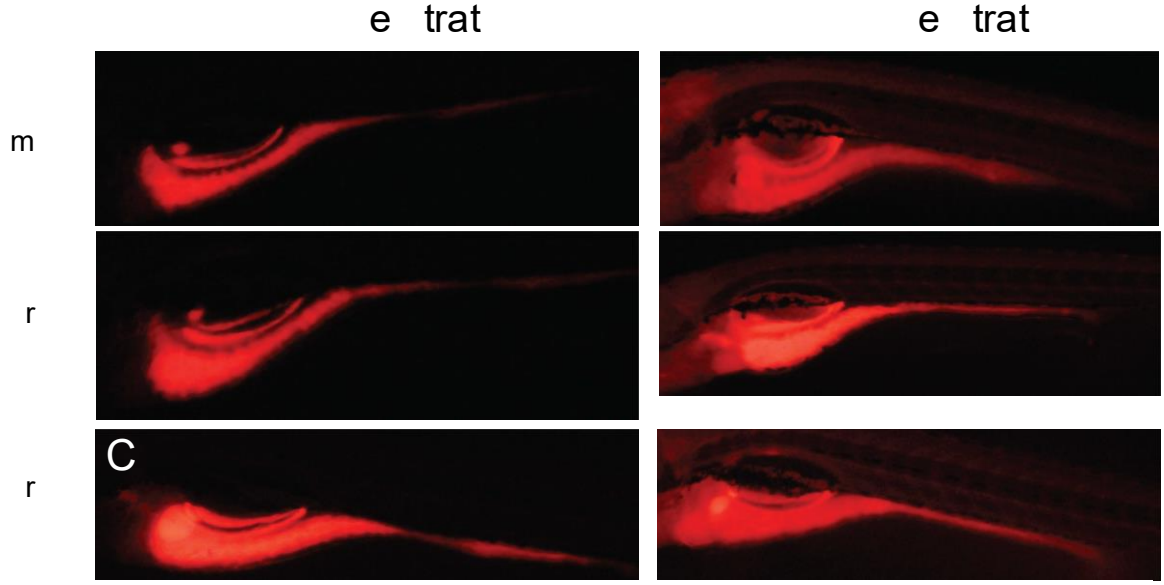

Figure 11. Concentration test for Nile Red dye. All larvae were incubated in Nile red medium for 16 hours before being washed and imaged. Larval zebrafish exposed to a low concentration of Nile red (0.0314 uM), (A) 30 minutes (n=5), (B) 4 hours (n=5), and (C) 6 hours (n=3) after being washed of excess Nile Red. A group of zebrafish kept in 0.314 µM Nile Red were also imaged (D) 30 minutes (n=5), (E) 4 hours (n=4), and (F) 6 hours (n=5) after washing. All larval heads are to the left of the images.

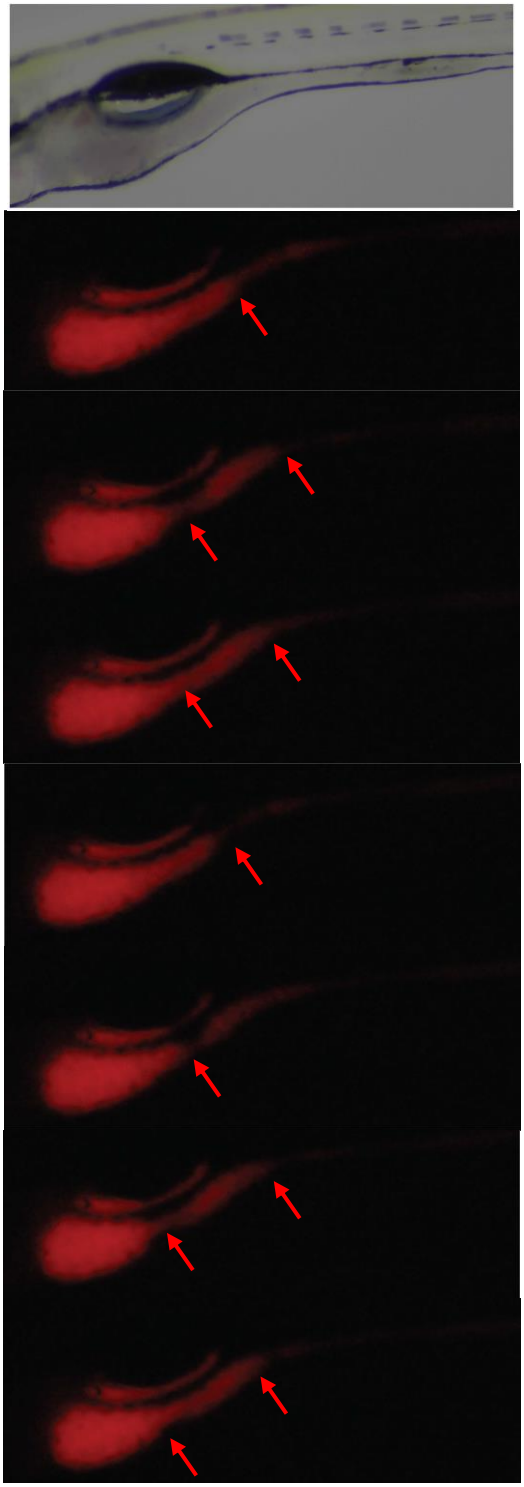

Figure 12. Visualization of contractions using Nile red dye. The series of images were taken of a single 9 dpf zebrafish 24 hours after being washed. Red arrows indicate the area of the intestinal bulb that is contracting. All larval heads are to the left of the images.

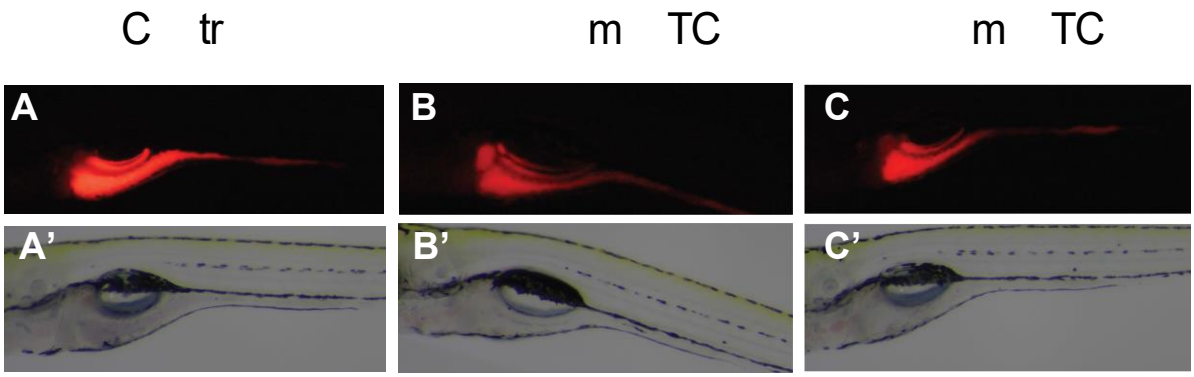

Figure 13. Pilot study for detecting an increase in intestinal transit rate with the treatment of transcinnamaldehyde (TC) using Nile red as a tracer. 7 dpf larvae were incubated in 0.0314 μM Nile red for 16 hours then washed. After washing, larvae were treated with (A, A') E3 medium (control), (B, B') 0.025 mM TC, or (C, C') 0.05 mM TC. (n=5 for all groups; only 1 trial was conducted). All images were of 7 dpf zebrafish and taken 6 hours after the treatment was given. All larval heads are to the left of the images. The student's t-test showed $p < 0.0005$ for control versus 0.05 mM TC, and $p < 0.005$ for control versus 0.025 mM TC.

Following the pilot study, the experiment was performed using nine dpf larvae and observations were extended to 24 hours. First, the effects of 0.05 mM TC were tested. As shown in Figure 14, there was a significant difference in the fluorescence intensity in the intestinal bulb between the TC-treated larvae compared to the controls.

Statistical analysis showed that at 6 hours post-treatment, the TC group had significantly less fluorescence than the controls at $p < 0.0005$. At 24 hours post-treatment, the difference between treated versus control larvae was $p < 0.005$.

Next, the experiment was performed using 0.025 mM TC. As predicted by the pilot study, this concentration was also effective, as shown in Figure 15. At six hours post-treatment, the TC-treated group had significantly less fluorescence intensity than the control group ($p < 0.005$). However, by 24 hours post-treatment, there was no difference between the groups ($p = 0.934$). From this set of experiments, I conclude that in zebrafish as in mammals, treatment with TC causes an increase in intestinal motility and thus faster intestinal transit.

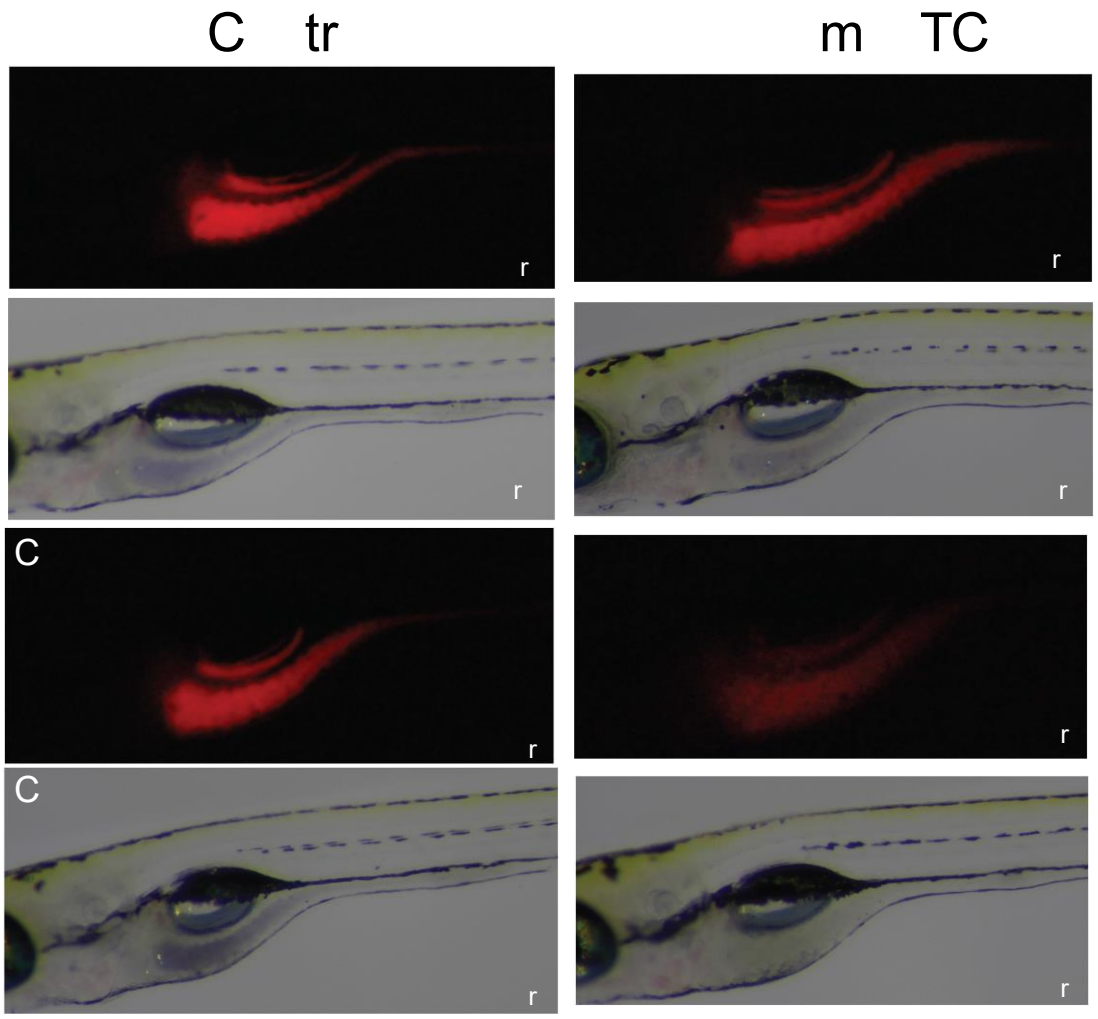

Figure 14. Treatment with 0.05 mM TC in the absence of other nutrients causes an increase in the intestinal transit rate. Larvae were incubated in 0.0314 μM Nile Red for 16 hours and then washed. After the wash, larvae were treated with (A, A', C, C') E3 medium (n=19 for 6 hours; n=20 for 24 hours) or (B, B', D, D') 0.05 mM TC (n=19 for 6 hours; n=20 for 24 hours) with images being taken 6 and 24 hours after administration of the treatment. All zebrafish were 9 dpf when TC was administered. All larval heads are to the left of the images. The student's t-test showed $p < 0.0005$ for control versus 0.05 mM TC after 6 hours and $p < 0.005$ for control versus 0.05 mM TC after 24 hours. All larval heads are to the left of the images.

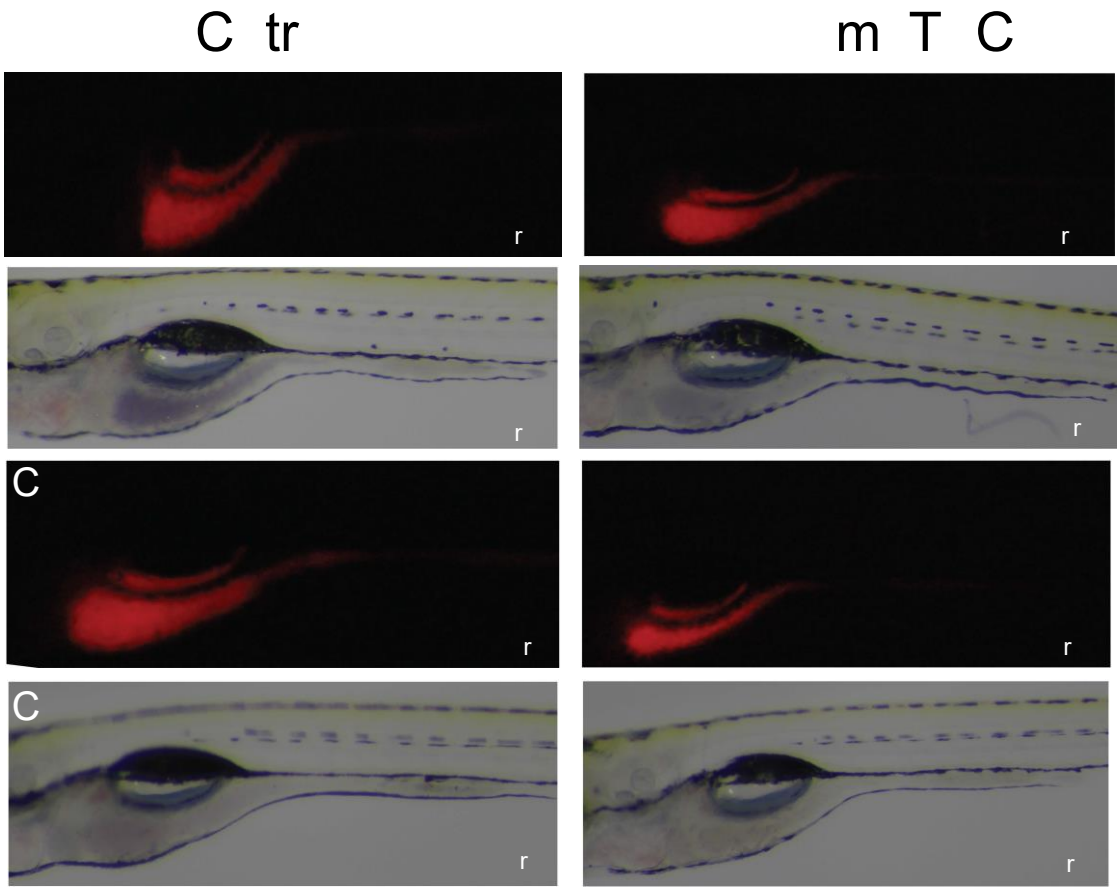

Figure 15. Treatment with 0.025 mM TC in the absence of other nutrients causes an increase in the intestinal transit rate Larvae were incubated in 0.0314 µM Nile Red for 16 hours and then washed. After the wash, larvae were treated with (A, A', C, C') E3 medium (n=19 for 6 hours; n=20 for 24 hours) or (B, B', D, D') 0.05 mM TC (n=19 for 6 hours; n=20 for 24 hours) with images being taken 6 and 24 hours after administration of the treatment. All zebrafish were 9 dpf when TC was administered. All larval heads are to the left of the images. The student's t-test showed $p < 0.005$ for control versus 0.025 mM TC, and $p=0.934$ for control versus 0.025 mM TC.

Discussion

Zebrafish are continuously being developed as a model organism to study human illnesses. The similar but simplistic layout of the zebrafish intestinal tract allows for relatively simple experimental designs (Figure 1). Zebrafish also share a high percent of genes with humans (Howe et al., 2013; Wallace et al., 2005). Gut transit assays have been developed in a variety of models to study specific aspects of intestinal function. These studies have been able to determine when coordinated and directional contractions appear. However, these studies used tracers that were not a normal part of the model organism's diet. While these studies provided very useful information it is also important to understand the functionality of the intestines in the presence of a natural food source. In order to do this, I helped develop an intestinal transit assay that used brine shrimp as the tracer. Using this assay, I was able to determine that temperature and the trpa1a agonist TC had an impact on the intestinal transit rate of larval zebrafish.

Functional studies

By using a digestible meal and controlled meal size I was able to determine that 9 dpf zebrafish typically empty their intestinal bulb within four hours of being fed. These results greatly vary from those of Field et al. (2009) who found that it took from 6 to over 24 hours for 7 dpf zebrafish to empty their intestinal bulb. Field et al. (2009) used dry food mixed with indigestible fluorescent polystyrene microspheres. I used brine shrimp which is a normal part of the zebrafish diet in the laboratory. Since larvae can digest brine it moves through the intestinal tract at a more precise rate. In the Field et al. (2009) experiments, the larvae were allowed to feed for one to two hours, and the amount consumed by each larva varied. By

contrast, for my experiments, the larvae were given only 15 minutes to feed to narrow the window of when digestion and excretion began. I have also previously shown that on 9 dpf or prior to 9 dpf larval zebrafish only consume a single brine shrimp (not shown).

Once it was determined that the intestinal assay developed by our lab could produce consistent results, I validated the assay by showing that it was able to detect decreased gut motility. By cooling the E3 medium that the larvae were in I was able to slow down the intestinal transit rate from 4 hours to approximately 7 hours after being fed. Since zebrafish are poikilotherms the metabolic rate is dependent on the temperature of the environment that they are in so it was expected that the intestinal transit rate would decrease when the temperature was decreased (Vergauwen et al., 2010). In further tests done in collaboration with others in the lab (not shown), treatment with $MgSO_4$ showed that the assay was able to detect increased gut motility. Thus, I concluded that the new assay was useful for studies of intestinal function. It is possible that the Trpa1 has a role in the change in intestinal transit time since in other model organisms, such as mice, it has been shown to be a temperature sensor (Karashima et al., 2009).

Once it was determined that the intestinal transit assay developed by the Kinkel Lab could differentiate between a normal and altered intestinal transit rate I sought to determine if an agonist of Trpa1a would increase the intestinal transit rate. Trpa1a is a nutrient receptor that is activated by the presence of TC. Taylor et al. (2017) previously used zebrafish to test the impact of 10 mM – 40 mM TC. These experiments determined that 10 mM TC was sufficient to reduce the amount of swimming done by the larvae. This was deemed a nociceptive response. The concentrations used in the experiments I conducted were 200 times lower (0.05 mM) and 400 times lower (0.025 mM) than those used by Taylor et al.

(2017) since the goal was to activate trpa1a channels without irritating the gut. However, it is still possible that there is a nociceptive response occurring. Bellono et al. (2017) proposed that TRPA1 receptors protect the submucosa in the intestinal bulb by stimulating faster intestinal transit in the presence of irritants, such as TC. However, these conclusions were drawn from studies conducted only in mammals. Based on the results from the experiments using brine shrimp as a meal, 0.05 mM TC was a high enough concentration to cause an increase in the intestinal transit rate of 9 dpf zebrafish. The larvae that were treated with 0.05 mM TC emptied their intestinal bulb roughly 1 hour faster than the control group.

Trpa1a studies

To determine how TC impacts the intestinal transit rate in the absence of other nutrients the fluorescent dye Nile red was used to fill the intestinal bulb. Zhou et al. (2014) used Nile red to determine how different drugs impacted the intestinal rate, so I followed a similar protocol with some minor altercations. I kept the larvae at a lower density to avoid causing them any stress. I did this by keeping them in small glass fish dishes instead of 6-well microplates. Treatment with Nile red alone enabled me to visualize intestinal contractions in live larvae. It is hypothesized that Nile red will activate stretch receptor without activating nutrient receptors. This suggests that activating stretch receptors may result in peristalsis. However, the observed contractions may have been produced by the migrating motility complex as part of normal inter-digestive phase contractions that occur between meals. More trials are needed to determine if there is any difference in the rate or directionality or timing of contractions between Nile red treated larvae and fasted larvae.

After the larvae were incubated in Nile red for 16 hours at a density of 5 fish per 5 mL E3 medium they were washed. The larvae were then treated with either 0.05 mM or 0.025 mM TC. The results indicate that both 0.025 mM TC and 0.05 mM TC are sufficient concentrations to increase the intestinal transit rate six hours after treatment. This was shown by a decrease in the intensity of Nile red remaining in the intestinal bulb when compared to controls. However, by 24 hours after treatment, only the larvae treated with 0.05 mM TC showed a significant further decrease in Nile red fluorescence intensity when compared to larvae imaged at six hours. These results indicate that 0.05 mM TC concentration has a longer-lasting impact on intestinal motility than the 0.025 mM TC concentration.

Since Nile red is a nonabsorbable tracer that only activates stretch receptors within the intestines it was expected that the transit rate would be slower when compared to brine shrimp. Brine shrimp have multiple nutrients present that likely activate more sensory receptors within the GI tract along with stretch receptors. The experiments I conducted focused on the intestinal bulb. It is likely that that the expression of different receptors, such as Trpa1a, within the intestinal bulb vary from the mid and distal intestine. If there are fewer or no Trpa1a receptors in the intestinal bulb then that could partially explain why the motility rate was much slower with the Nile red than with brine shrimp. Determining the expression pattern of *trpa1a* will be important for determining if this is the case.

Expression pattern studies

The expression pattern of some genes within the zebrafish GI tract have already been defined. The genes ada, slc10a2, and aqp4 are known to be expressed only in the intestinal bulb, mid-intestine, and distal intestine, respectively (Table 3) (Thisse and Thisse, 2004;

Tingaud-Sequeira et al., 2010). These genes can be utilized as control genes when determining the expression patterns of ano1, kita, trpa1a, and trpa1b using RT-PCR. Kita and ano1 are known to be required for the proper development and function of ICCs (Rich et al., 2013; Uyttebroek et al., 2013). The paralogs of the human gene TRPA1, Trpa1a and Trpa1b, are known to be activated by TC and mustard oil, respectively. Since there are known agonists for these receptors the way in which they impact intestinal motility through possible indirect signaling to the ICCs and smooth muscle can be studied. Further understanding of the expression patterns of these genes should lead to a more comprehensive model for how slow waves are controlled by ICC. These patterns could be determined by utilizing RT-PCR, immunohistochemistry, and *in situ* hybridization at different developmental timepoints.

An outstanding question in the field is what is the mechanism that controls the pace of the slow wave in ICC. I propose that a negative feedback loop is initiated when PIP_2 is hydrolyzed to produce the IP_3 that triggers Ca^{2+} release from the ER (Figure 16). PIP_2 stabilizes the open conformation of ano1 but as PIP_2 is hydrolyzed, there is less PIP_2 present to maintain the open state. Activation of phosphatidylinositol phosphate (PIP) kinases is needed to produce PIP_2 by phosphorylating PIP (Legate et al., 2012). Simultaneously, a positive feedback loopback loop is occurring with Ca^{2+}. As more Ca^{2+} is released from the ER, VDCCs open allowing an influx of Ca^{2+} into the cell. However, as there is less PIP_2 available due to it being hydrolyzed by PLC, the concentration of Ca^{2+} becomes irrelevant for the activation of ano1 due to the Ca^{2+} desensitization that occurs without PIP_2. The mechanism that leads to the activation of PIP kinases, and therefore replenishment of PIP_2 stores, does not appear to be known. It is known that PIP kinases localize in different regions of the cells and therefore PIP_2 has specific regions it pools in as well. Whether or not PIP_2

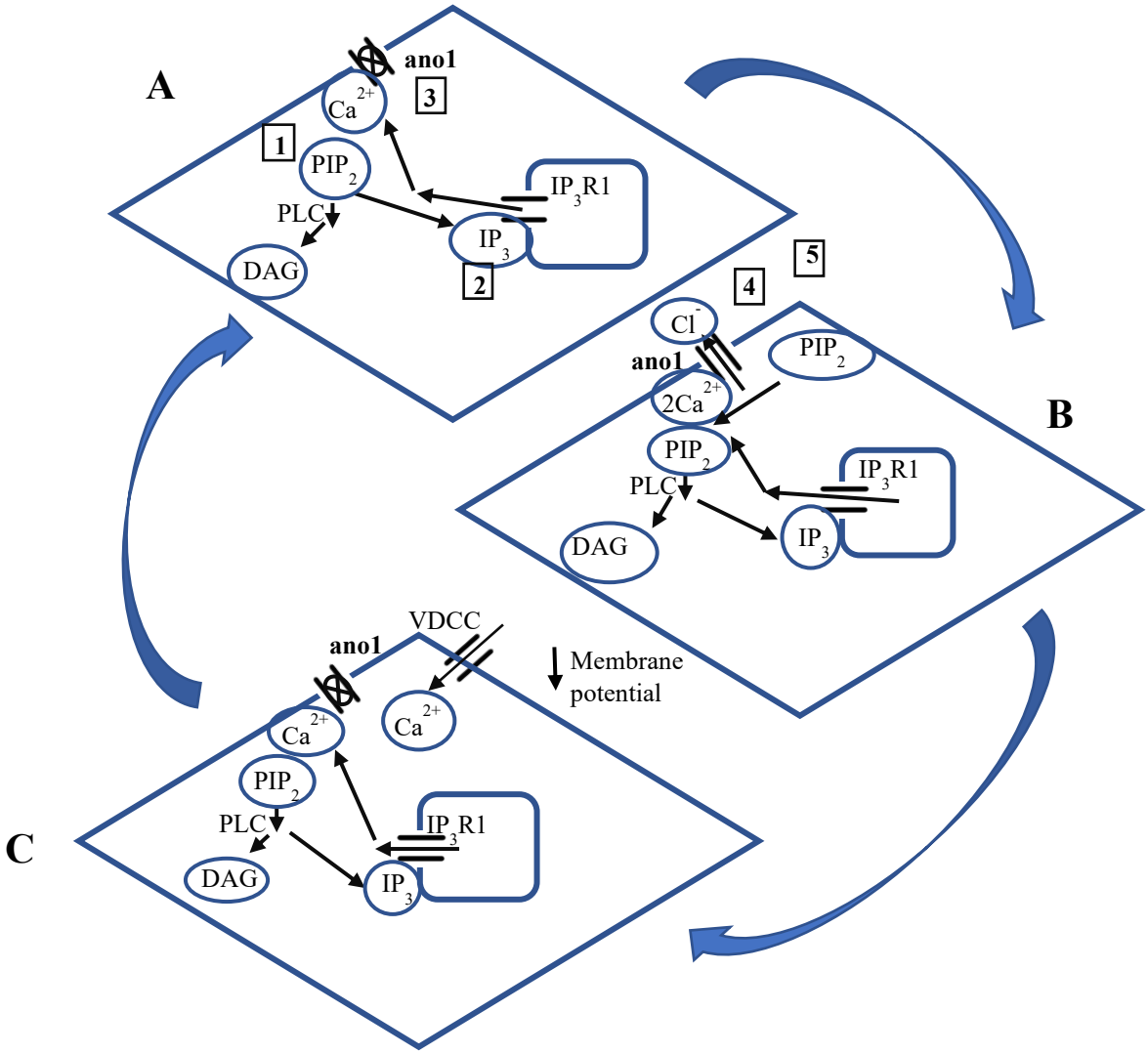

Figure 16. Proposed model for the mechanism that controls ICC slow wave frequency. A) Calcium release results in partial opening of the ano1 transmembrane channel. Step 1. PIP_2 is hydrolyzed by phospholipase C (PLC) producing diacylglycerol (DAG) and inositol 1,4,5-triphosphophate (IP_3). Step 2. IP_3 binding to IP_3R1 leads to the release of Ca^{2+} from the endoplasmic reticulum. Step 3. Ca^{2+} binds to ano1 causing it to partially open. B) Calcium binding is stabilized. Step 4. PIP_2 binds to ano1 stabilizing the interaction between Ca^{2+} and ano1, allowing anot1 to stay open. Step 5. As PIP_2 continues to be hydrolyzed by PLC, its concentration dwindles and less is available for the stabilization of Ca^{2+} and ano1. C) Membrane potential change. When Ano1 opens there is an efflux of negatively charged Cl^- out the cells that triggers voltage-gated Ca^{2+} channels (VDCC) to open leading to an even higher concentration of Ca^{2+} in the cell. As PIP_2 is hydrolyzed there is less available to stabilize the interaction between Ca^{2+} and ano1 which leads to Ca^{2+} desensitization. As this occurs ano1 closes and the cycles starts again.

pools are localized in regions where ano1 is expressed on the membrane of ICC does not appear to be known. While the current evidence supports this hypothesis, some type of immunostaining is still needed to provide direct evidence.

Future Directions

A better understanding of what channels are present on the different intestinal cell types and how those channels are controlled is needed. The experiments in this thesis laid the groundwork for future studies of intestinal development and function. There are different transgenic lines of fish that could potentially be used with particle image velocimetry (PIV) to allow the software to focus on the intestinal wall when there is food in the intestinal lumen. PIV allows for the amplitude, velocity, and frequency of contractions to be determined using larvae that have empty intestines. *Tg(sm22α-b: GFP)* is a transgenic line that fluorescently tags cells that have fully committed to being iSM cells (Seiler et al., 2010). Combining this fish line with PIV could potentially allow for intestinal motility with a bolus present to be tracked. PIV that uses wildtype zebrafish cannot distinguish between a bolus and the intestinal smooth muscle. It may be possible to program the software to distinguish between a bolus and the intestinal smooth muscle if there was more of a contrast between them. Since contraction patterns are expected to be different between fish with empty intestinal lumens and those with contents in their intestinal lumen, developing a technique that allows both to be analyzed would allow for the whole picture of intestinal motility to be captured (Won et al., 2005). If this technique is possible, when targeting different receptors within the GI tract of zebrafish with various agonists and antagonists it would be possible to tell precisely what is being impacted. In order to do this a more comprehensive understanding of ion channel expression is needed.

What is known about the ion channels expressed on the ICC within the zebrafish GI tract is extremely limited. While it is well known that ano1 is present on the ICC of zebrafish no other ionic channels have been investigated (Uyttebroek et al., 2013). Many ion channels

have been well studied in the heart of zebrafish and could provide a starting point when beginning this investigation in the intestines. Considering the similarities between the human and zebrafish genome there is a high probability for many similarities in the ion channel expression of ICC (Howe et al., 2013).

Though ano1 is one of the most highly studied channels on ICCs, there is still much that needs to be understood before a full picture of the role ano1 plays in intestinal motility is put together. ICCs are present in other organs such as the urethra and pancreas, however, the presence of ano1 does not appear to be a research area of interest for these organs. By contrast, there is a plethora of research examining ano1 in respiratory epithelium and smooth muscle cells because of the potential for targeting this receptor to treat cystic fibrosis and asthma (Danielsson et al., 2015; Ji et al., 2019). The current understanding of how ano1 functions on ICCs in the GI tract supports that ano1 is important for proper intestinal function. The signaling pathway/loop controlling activation and inhibition of ano1 has not been defined yet and may provide a much-needed therapeutic target for treating a variety of GI tract diseases.

Works Cited

Ambache, N. (1947). The electrical activity of isolated mammalian intestines. *J Physiol* **106**, 139–153.

Aslanidi, O. V., Sleiman, R. N., Boyett, M. R., Hancox, J. C. and Zhang, H. (2010). Ionic mechanisms for electrical heterogeneity between rabbit purkinje fiber and ventricular cells. *Biophys J* **98**, 2420–2431.

Aslanidi, O. V., Colman, M. A., Stott, J., Dobrzynski, H., Boyett, M. R., Holden, A. V. and Zhang, H. (2011). 3D virtual human atria: A computational platform for studying clinical atrial fibrillation. *Prog Biophys Mol Biol* **107**, 156–168.

Atkinson, A., Inada, S., Li, J., Tellez, J. O., Yanni, J., Sleiman, R., Allah, E. A., Anderson, R. H., Zhang, H., Boyett, M. R., et al. (2011). Anatomical and molecular mapping of the left and right ventricular His–Purkinje conduction networks. *J Mol Cell Cardiol* **51**, 689–701.

Bader, C. R., Bertrand, D. and Schwartz, E. A. (1982). Voltage-activated and calcium-activated currents studied in solitary rod inner segments from the salamander retina. *J Physiol* **331**, 253–284.

Baker, S. A., Drumm, B. T., Cobine, C. A., Keef, K. D. and Sanders, K. M. (2018). Inhibitory neural regulation of the Ca2+ transients in intramuscular interstitial cells of Cajal in the small intestine. *Front Physiol* **9**, 238.

Bao, R., Lifshitz, L. M., Tuft, R. A., Bellvé, K., Fogarty, K. E. and ZhuGe, R. (2008). A close association of RyRs with highly dense clusters of ca2+-activated cl− channels underlies the activation of stics by ca2+ sparks in mouse airway smooth muscle. *J Gen Physiol* **132**, 145–160.

Baruscotti, M., Barbuti, A. and Bucchi, A. (2010). The cardiac pacemaker current. *J Mol Cell Cardiol* **48**, 55–64.

Bellono, N. W., Bayrer, J. R., Leitch, D. B., Castro, J., Zhang, C., O'Donnell, T., Brierley, S. M., Ingraham, H. A. and Julius, D. (2017). Enterochromaffin cells are gut chemosensors that couple to sensory neural pathways. *Cell* **170**, 185–198.

Berg, J., Yang, H. and Jan, L. Y. (2012). Ca2+-activated Cl− channels at a glance. *J Cell Sci* **125**, 1367–1371.

Berridge, M. J., Lipp, P. and Bootman, M. D. (2000). The versatility and universality of calcium signalling. *Nat Rev Mol Cell Biol* **1**, 11–21.

Blair, P. J., Rhee, P.-L., Sanders, K. M. and Ward, S. M. (2014). The significance of interstitial cells in neurogastroenterology. *J Neurogastroenterol Motil* **20**, 294–317.

Bogdanov KY., Vinogradova Tatiana M. and Lakatta Edward G. (2001). Sinoatrial nodal cell ryanodine receptor and Na+-Ca2+ exchanger. *Circ Res* **88**, 1254–1258.

Bulley, S. A., Neeb Zachary P., Burris Sarah K., Bannister John P., Thomas-Gatewood Candice M., Jangsangthong Wanchana and Jaggar Jonathan H. (2012). TMEM16A/ANO1 channels contribute to the myogenic response in cerebral arteries. *Circ Res* **111**, 1027–1036.

Burns, A. J. (2007). Disorders of interstitial cells of Cajal. *J. Pediatr. Gastroenterol. Nutr.* **45**, S103–S106.

Caputo, A., Caci, E., Ferrera, L., Pedemonte, N., Barsanti, C., Sondo, E., Pfeffer, U., Ravazzolo, R., Zegarra-Moran, O. and Galietta, L. J. V. (2008). TMEM16A, a membrane protein associated with calcium-dependent chloride channel activity. *Science* **322**, 590–594.

Chandler, N. J., Sharma, V., Sigg, D. C., Boyett, M. R., Dobrzynski, H., Difrancesco, D., Baruscotti, M., Longhi, R., Anderson, R. H., Billeter, R., et al. (2009). Molecular Architecture of the Human Sinus Node Insights Into the Function of the Cardiac Pacemaker. *Circulation* 1562–1575.

Chen, H., Ördög, T., Chen, J., Young, D. L., Bardsley, M. R., Redelman, D., Ward, S. M. and Sanders, K. M. (2007). Differential gene expression in functional classes of interstitial cells of Cajal in murine small intestine. *Physiol Genomics* **31**, 492–509.

Chevalier, N. R., Fleury, V., Dufour, S., Proux-Gillardeaux, V. and Asnacios, A. (2017). Emergence and development of gut motility in the chicken embryo. *PLOS ONE* **12**, e0172511.

Chevalier, N. R., Dacher, N., Jacques, C., Langlois, L., Guedj, C. and Faklaris, O. (2019). Embryogenesis of the peristaltic reflex. *J Physiol* **597**, 2785–2801.

Cloney, K., Steele, S. L., Stoyek, M. R., Croll, R. P., Smith, F. M., Prykhozhij, S. V., Brown, M. M., Midgen, C., Blake, K. and Berman, J. N. (2018). Etiology and functional validation of gastrointestinal motility dysfunction in a zebrafish model of CHARGE syndrome. *FEBS J* **285**, 2125–2140.

Coppen, S. R. and Severs, N. J. (2002). Diversity of Connexin Expression Patterns in the Atrioventricular Node: Vestigial Consequence or Functional Specialization? *J Cardiovasc Electrophysiol* **13**, 625–626.

Coppen, S. R., Severs, N. J. and Gourdie, R. G. (1999). Connexin45 (α6) expression delineates an extended conduction system in the embryonic and mature rodent heart. *Dev Genet* **24**, 82–90.

Corey, D. P., García-Añoveros, J., Holt, J. R., Kwan, K. Y., Lin, S.-Y., Vollrath, M. A., Amalfitano, A., Cheung, E. L.-M., Derfler, B. H., Duggan, A., et al. (2004).

TRPA1 is a candidate for the mechanosensitive transduction channel of vertebrate hair cells. *Nature* **432**, 723–730.

Cousins, H. M., Edwards, F. R., Hickey, H., Hill, C. E. and Hirst, G. D. S. (2003). Electrical coupling between the myenteric interstitial cells of Cajal and adjacent muscle layers in the guinea-pig gastric antrum. *J Physiol* **550**, 829–844.

Daniel, E. E., Wang, Y.-F. and Cayabyab, F. S. (1998). Role of gap junctions in structural arrangements of interstitial cells of Cajal and canine ileal smooth muscle. *Am J Physiol Gastrointest Liver Physiol* **274**, G1125–G1141.

Danielsson, J., Perez-Zoghbi, J., Bernstein, K., Barajas, M. B., Zhang, Y., Kumar, S., Sharma, P. K., Gallos, G. and Emala, C. W. (2015). Antagonists of the TMEM16A calcium-activated chloride channel codulate airway smooth muscle tone and intracellular calcium. *Anesthesiology* **123**, 569–581.

Dobrzynski, H., Nikolski, V. P., Sambelashvili, A. T., Greener, I. D., Yamamoto, M., Boyett, M. R. and Efimov, I. R. (2003). Site of origin and molecular substrate of atrioventricular junctional rhythm in the rabbit heart. *Circ Res* **93**, 1102–1110.

Dobrzynski, H., Anderson, R. H., Atkinson, A., Borbas, Z., D'Souza, A., Fraser, J. F., Inada, S., Logantha, S. J. R. J., Monfredi, O., Morris, G. M., et al. (2013). Structure, function and clinical relevance of the cardiac conduction system, including the atrioventricular ring and outflow tract tissues. *Pharmacol Therpeut* **139**, 260–288.

Drumm, B. T., Large, R. J., Hollywood, M. A., Thornbury, K. D., Baker, S. A., Harvey, B. J., McHale, N. G. and Sergeant, G. P. (2015). The role of Ca2+ influx in spontaneous Ca2+ wave propagation in interstitial cells of Cajal from the rabbit urethra. *J Physiol* **593**, 3333–3350.

Drumm, B. T., Hennig, G. W., Battersby, M. J., Cunningham, E. K., Sung, T. S., Ward, S. M., Sanders, K. M. and Baker, S. A. (2017). Clustering of Ca2+ transients in interstitial cells of Cajal defines slow wave duration. *J Gen Physiol* **149**, 703–725.

Drumm, B. T., Hwang, S. J., Baker, S. A., Ward, S. M. and Sanders, K. M. (2019a). Ca2+ signalling behaviours of intramuscular interstitial cells of Cajal in the murine colon. *J Physiol* **597**, 3587–3617.

Drumm, B. T., Rembetski, B. E., Baker, S. A. and Sanders, K. M. (2019b). Tonic inhibition of murine proximal colon is due to nitrergic suppression of Ca2+ signaling in interstitial cells of Cajal. *Sci Rep* **9**, 4402.

Eames Nalle, S. C., Franse, K. F. and Kinkel, M. D. (2017). Chapter 11 - Analysis of pancreatic disease in zebrafish. In *Methods in Cell Biology* (ed. Detrich, H. W.), Westerfield, M.), and Zon, L. I.), pp. 271–295. Academic Press.

Faussone-Pellegrini, M.-S., Romagnoli, P. and Cortesini, C. (1977). The ultrastructure of the muscle coat of human gastro-oesophageal junction, with special reference to "interstitial cells of Cajal"†. *J Anat Embryol* **7**, 1–8.

Field, H. A., Kelley, K. A., Martell, L., goldstein, A. M. and Serluca, F. C. (2009). Analysis of gastrointestinal physiology using a novel intestinal transit assay in zebrafish. *Neurogastroenterol. Motil.* **21**, 304–312.

Ganz, J., Baker, R. P., Hamilton, M. K., Melancon, E., Diba, P., Eisen, J. S. and Parthasarathy, R. (2018). Image velocimetry and spectral analysis enable quantitative characterization of larval zebrafish gut motility. *Neurogastroenterol Motil* **30**, e13351.

Gourdie, R. G., Severs, N. J., Green, C. R., Rothery, S., Germroth, P. and Thompson, R. P. (1993). The spatial distribution and relative abundance of gap-junctional connexin40 and connexin43 correlate to functional properties of components of the cardiac atrioventricular conduction system. *J Cell Sci* 985–991.

Grant, A. O., Carboni, M. P., Neplioueva, V., Starmer, C. F., Memmi, M., Napolitano, C. and Priori, S. (2002). Long QT syndrome, Brugada syndrome, and conduction system disease are linked to a single sodium channel mutation. *J Clin Invest* **110**, 1201–1209.

Greener, I. D., Monfredi, O., Inada, S., Chandler, N. J., Tellez, J. O., Atkinson, A., Taube, M.-A., Billeter, R., Anderson, R. H. and Efimov, I. R. (2011). Molecular architecture of the human specialised atrioventricular conduction axis. *J Mol Cell Cardiol* **50**, 642–651.

Hartzell, C., Putzier, I. and Arreola, J. (2005). Calcium-activated chloride channels. *Annu Rev Physiol* **67**, 719–758.

Hatton, W. J., Mason, H. S., Carl, A., Doherty, P., Latten, M. J., Kenyon, J. L., Sanders, K. M. and Horowitz, B. (2001). Functional and molecular expression of a voltage-dependent K+ channel (Kv1.1) in interstitial cells of Cajal. *J Physiol* **533**, 315–327.

Heanue, T. A., Boesmans, W., Bell, D. M., Kawakami, K., Berghe, P. V. and Pachnis, V. (2016). A novel zebrafish ret heterozygous model of Hirschsprung disease identifies a functional role for mapk10 as a modifier of enteric nervous system phenotype severity. *PLOS Genet* **12**, e1006439.

Holmberg, A., Olsson, C. and Hennig, G. W. (2007). TTX-sensitive and TTX-insensitive control of spontaneous gut motility in the developing zebrafish (Danio rerio) larvae. *J Exp Biol* **210**, 1084–1091.

Howe, K., Clark, M. D., Torroja, C. F., Torrance, J., Berthelot, C., Muffato, M., Collins, J. E., Humphray, S., McLaren, K., Matthews, L., et al. (2013). The zebrafish reference genome sequence and its relationship to the human genome. *Nature* **496**, 498–503.

Huang, F., Zhang, H., Wu, M., Yang, H., Kudo, M., Peters, C. J., Woodruff, P. G., Solberg, O. D., Donne, M. L., Huang, X., et al. (2012). Calcium-activated chloride channel TMEM16A modulates mucin secretion and airway smooth muscle contraction. *PNAS* **109**, 16354–16359.

Huizinga, J. D., Chen, J.-H., Mikkelsen, H. B., Wang, X.-Y., Parsons, S. P. and Zhu, Y. F. (2013). Interstitial cells of Cajal, from structure to function. *Front Neurosci* **7**,.

Hwang, S. J., Blair, P. J. A., Britton, F. C., O'Driscoll, K. E., Hennig, G., Bayguinov, Y. R., Rock, J. R., Harfe, B. D., Sanders, K. M. and Ward, S. M. (2009). Expression of anoctamin 1/TMEM16A by interstitial cells of Cajal is fundamental for slow wave activity in gastrointestinal muscles. *J Physiol* **587**, 4887–4904.

Iino, S., Horiguchi, K., Horiguchi, S. and Nojyo, Y. (2009). c-Kit-negative fibroblast-like cells express platelet-derived growth factor receptor α in the murine gastrointestinal musculature. *Histochem Cell Biol* **131**, 691–702.

Jain, D., Moussa, K., Tandon, M., Culpepper-morgan, J. and Proctor, D. D. (2003). Role of interstitial cells of Cajal in motility disorders of the bowel. *Am. J. Gastroenterol.* **98**, 618–624.

Ji, Q., Guo, S., Wang, X., Pang, C., Zhan, Y., Chen, Y. and An, H. (2019). Recent advances in TMEM16A: Structure, function, and disease. *J Cell Physiol* **234**, 7856–7873.

Jiang, P., Hou, Y., Fu, W., Tao, X., Luo, J., Lu, H., Xu, Y., Han, B. and Zhang, J. (2018). Characterization of lncRNAs involved in cold acclimation of zebrafish ZF4 cells. *PLOS ONE* **13**, e0195468.

Jiménez, M., Borderies, J. R., Vergara, P., Wang, Y.-F. and Daniel, E. E. (1999). Slow waves in circular muscle of porcine ileum: structural and electrophysiological studies. *Am J Physiol Gastrointest Liver Physiol* **276**, G393–G406.

Jin, X., Shah, S., Liu, Y., Zhang, H., Lees, M., Fu, Z., Lippiat, J. D., Beech, D. J., Sivaprasadarao, A., Baldwin, S. A., et al. (2013). Activation of the Cl− channel Ano1 by localized calcium signals in nociceptive sensory neurons requires coupling with the IP3 receptor. *Sci Signal* **6**, ra73.

Jin, X., Shah, S., Du, X., Zhang, H. and Gamper, N. (2016). Activation of Ca2+-activated Cl− channel ANO1 by localized Ca2+ signals. *J Physiol* **594**, 19–30.

Joung, B., Ogawa, M., Lin, S.-F. and Chen, P.-S. (2009). The calcium and voltage clocks in sinoatrial node automaticity. *Korean Circ J* **39**, 217–222.

Karashima, Y., Talavera, K., Everaerts, W., Janssens, A., Kwan, K. Y., Vennekens, R., Nilius, B. and Voets, T. (2009). TRPA1 acts as a cold sensor in vitro and in vivo. *PNAS* **106**, 1273–1278.

Kim, T. W., Koh, S. D., Ördög, T., Ward, S. M. and Sanders, K. M. (2003). Muscarinic regulation of pacemaker frequency in murine gastric interstitial cells of Cajal. *J Physiol* **546**, 415–425.

Kito, Y., Fukuta, H. and Suzuki, H. (2002). Components of pacemaker potentials recorded from the guinea pig stomach antrum. *Pflugers Arch* **445**, 202–217.

Kito, Y., Ward, S. M. and Sanders, K. M. (2005). Pacemaker potentials generated by interstitial cells of Cajal in the murine intestine. *Am J Physiol Cell Physiol* **288**, C710–C720.

Koh, S. D. and Rhee, P.-L. (2013). Ionic Conductance(s) in Response to Post-junctional Potentials. *J Neurogastroenterol Motil* **19**, 426–432.

Koh, S. D., Sanders, K. M. and Ward, S. M. (1998). Spontaneous electrical rhythmicity in cultured interstitial cells of Cajal from the murine small intestine. *J Physiol* **513**, 203–213.

Kuhlman, J. and Eisen, J. S. (2007). Genetic screen for mutations affecting development and function of the enteric nervous system. *Dev Dyn* **236**, 118–127.

Kurahashi, M., Zheng, H., Dwyer, L., Ward, S. M., Koh, S. D. and Sanders, K. M. (2011). A functional role for the 'fibroblast-like cells' in gastrointestinal smooth muscles. *J Physiol* **589**, 697–710.

Kuruma, A. and Hartzell, H. C. (2000). Bimodal Control of a Ca2+-Activated Cl− Channel by Different Ca2+ Signals. *J Gen Physiol* **115**, 59–80.

Lakatta, E. G. and DiFrancesco, D. (2009). JMCC Point-Counterpoint. *J Mol Cell Cardiol* **47**, 157–170.

Langton, P., Ward, S. M., Carl, A., Norell, M. A. and Sanders, K. M. (1989). Spontaneous electrical activity of interstitial cells of Cajal isolated from canine proximal colon. *Proc Natl Acad Sci U S A* **86**, 7280–7284.

Le, S. C., Jia, Z., Chen, J. and Yang, H. (2019). Molecular basis of PIP 2 -dependent regulation of the Ca 2+ -activated chloride channel TMEM16A. *Nat Commun* **10**, 3769.

Legate, K. R., Montag, D., Bottcher, R. T., Takahashi, S. and Fassler, R. (2012). Comparative phenotypic analysis of the two major splice isoforms of phosphatidylinositol phosphate kinase type I in vivo. *J Cell Sci* **125**, 5636–5646.

Lickwar, C. R., Camp, J. G., Weiser, M., Cocchiaro, J. L., Kingsley, D. M., Furey, T. S., Sheikh, S. Z. and Rawls, J. F. (2017). Genomic dissection of conserved transcriptional regulation in intestinal epithelial cells. *PLOS Biology* **15**, e2002054.

Lyford, G. L. and Farrugia, G. (2003). Ion channels in gastrointestinal smooth muscle and interstitial cells of Cajal. *Curr Opin Pharmacol* **3**, 583–587.

Maeda, H., Yamagata, A., Nishikawa, S., Yoshinaga, K., Nishi, K. and Nishikawa, S.-I. (1992). Requirement of c-kit for development of intestinal pacemaker system. *Development* **116**, 369–375.

Meijler, F. L. and Janse, M. J. (1988). Morphology and electrophysiology of the mammalian atrioventricular node. *Physiol. Rev.* **68**, 608–647.

Moe, G. K., Preston, J. B. and Burlington, H. (1956). Physiologic evidence for a dual A-V transmission system. *Circ Res* **4**, 357–375.

Monfredi, O., Dobrzynski, H., Mondal, T., Boyett, M. R. and Morris, G. M. (2010). The anatomy and physiology of the sinoatrial node—a contemporary review. *Pacing Clin Electrophysiol* **33**, 1392–1406.

Norton, A., Franse, K. F., Daw, T., Gordon, L., Vitiello, P. F. and Kinkel, M. D. (2019). Larval rearing methods for small-scale production of healthy zebrafish. *East Biol* **2019**, 33–46.

Ohkawa, H. and Watanabe, M. (1977). Effects of gastrointestinal hormones on the electrical and mechanical activities of the cat small intestine. *Jpn J Physiol* **27**, 71–79.

Olden, T., Akhtar, T., Beckman, S. A. and Wallace, K. N. (2008). Differentiation of the zebrafish enteric nervous system and intestinal smooth muscle. *Genesis* **46**, 484–498.

Padmanabhan, P., Grosse, J., Asad, A. B. M. A., Radda, G. K. and Golay, X. (2013). Gastrointestinal transit measurements in mice with 99mTc-DTPA-labeled activated charcoal using NanoSPECT-CT. *EJNMMI Res* **3**, 60.

Parichy, D. M., Elizondo, M. R., Mills, M. G., Gordon, T. N. and Engeszer, R. E. (2009). Normal table of postembryonic zebrafish development: Staging by externally visible anatomy of the living fish. *Developmental Dynamics* **238**, 2975–3015.

Parkman, H. P. and Doma, S. (2006). Importance of gastrointestinal motility disorders. *Pract. Gastroenterol.* **1**, 23–40.

Paulino, C., Neldner, Y., Lam, A. K., Kalienkova, V., Brunner, J. D., Schenck, S. and Dutzler, R. (2017a). Structural basis for anion conduction in the calcium-activated chloride channel TMEM16A. *eLife* **6**, e26232.

Paulino, C., Kalienkova, V., Lam, A. K. M., Neldner, Y. and Dutzler, R. (2017b). Activation mechanism of the calcium-activated chloride channel TMEM16A revealed by cryo-EM. *Nature* **552**, 421–425.

Pedemonte, N. and Galietta, L. J. V. (2014). Structure and function of TMEM16 proteins (anoctamins). *Physiol Rev* **94**, 419–459.

Peters, C. J., Gilchrist, J. M., Tien, J., Bethel, N. P., Qi, L., Chen, T., Wang, L., Jan, Y. N., Grabe, M. and Jan, L. Y. (2018). The sixth transmembrane segment is a major gating component of the TMEM16A calcium-activated chloride channel. *Neuron* **97**, 1063–1077.

Prober, D. A., Zimmerman, S., Myers, B. R., McDermott, B. M., Kim, S.-H., Caron, S., Rihel, J., Solnica-Krezel, L., Julius, D., Hudspeth, A. J., et al. (2008). Zebrafish trpa1 channels are required for chemosensation but not for thermosensation or mechanosensory hair cell function. *J. Neurosci.* **28**, 10102–10110.

Rich, A., Leddon, S. A., Hess, S. L., Gibbons, S. J., Miller, S., Xu, X. and Farrugai, G. (2007). Kit-like immunoreactivity in the zebrafish gastrointestinal tract reveals putative ICC. *Dev Dyn* **236**, 903–911.

Rich, A., Gordon, S., Brown, C., Gibbons, S. J., Schaefer, K., Hennig, G. and Farrugia, G. (2013). Kit signaling is required for development of coordinated motility patterns in zebrafish gastrointestinal tract. *Zebrafish* **10**, 154–160.

Roberts, R. R., Ellis, M., Gwynne, R. M., Bergner, A. J., Lewis, M. D., Beckett, E. A., Bornstein, J. C. and Young, H. M. (2010). The first intestinal motility patterns in fetal mice are not mediated by neurons or interstitial cells of Cajal. *J Physiol* **588**, 1153–1169.

Sanders, K. M., Koh, S. D., Ro, S. and Ward, S. M. (2012). Regulation of gastrointestinal motility—insights from smooth muscle biology. *Nat Rev Gastroenterol Hepatol* **9**, 633–645.

Sanders, K. M., Ward, S. M. and Koh, S. D. (2014). Interstitial cells: Regulators of smooth muscle function. *Physiol Rev* **94**, 859–907.

Sarna, S. K. (2010). *Colonic motility: From benchside to bedside.* Morgan & Claypool Life Sciences.

Schroeder, B. C., Cheng, T., Jan, Y. N. and Jan, L. Y. (2008). Expression cloning of TMEM16A as a calcium-activated chloride channel subunit. *Cell* **134**, 1019–1029.

Seiler, C., Abrams, J. and Pack, M. (2010). Characterization of zebrafish intestinal smooth muscle development using a novel sm22α-b promoter. *Dev Dyn* **239**, 2806–2812.

Shepherd, I. and Eisen, J. (2011). Development of the zebrafish enteric nervous system. *Methods Cell Biol* **101**, 143–160.

Sherwood, L. and Cengage Learning (Firm) (2013). *Human physiology: from cells to systems*. Belmont, CA: Brooks/Cole, Cengage Learning.

Shin Y., Dobrzynski H., Fedorov F., Xu SZ, Yamanushi Tomoko T., Jones SA., Yamamoto M., Nikolski VP., Efimov IR. and Boyett MR. (2006). Localization of

na+ channel isoforms at the atrioventricular junction and atrioventricular node in the rat. *Circulation* **114**, 1360–1371.

Singh, R. D., Gibbons, S. J., Saravanaperumal, S. A., Du, P., Hennig, G. W., Eisenman, S. T., Mazzone, A., Hayashi, Y., Cao, C., Stoltz, G. J., et al. (2014). Ano1, a Ca2+-activated Cl− channel, coordinates contractility in mouse intestine by Ca2+ transient coordination between interstitial cells of Cajal. *J Physiol* **592**, 4051–4068.

Spach, M. S., Barr, R. C., Serwer, G. S., Johnson, E. A. and Kootsey, J. M. (1971). Collision of excitation waves in the dog purkinje system: extracellular identification. *Circ Res* **29**, 499–511.

Strege, P. R., Ou, Y., Sha, L., Rich, A., Gibbons, S. J., Szurszewski, J. H., Sarr, M. G. and Farrugia, G. (2003). Sodium current in human intestinal interstitial cells of Cajal. *Am J Physiol Gastrointest Liver Physiol* **285**, G1111–G1121.

Suzuki, N., Prosser, C. L. and Dahms, V. (1986). Boundary cells between longitudinal and circular layers: essential for electrical slow waves in cat intestine. *APS* G287–G294.

Taylor, J. C., Dewberry, L. S., Totsch, S. K., Yessick, L. R., DeBerry, J. J., Watts, S. A. and Sorge, R. E. (2017). A novel zebrafish-based model of nociception. *Physiology & Behavior* **174**, 83–88.

Thisse, B. and Thisse, C. (2004). Fast Release Clones: A High Throughput Expression Analysis. *ZFIN direct data submission*.

Thuneberg, L. (1999). One hundred years of interstitial cells of Cajal. *Microsc Res Tech* **47**, 223–238.

Tingaud-Sequeira, A., Calusinska, M., Finn, R. N., Chauvigné, F., Lozano, J. and Cerdà, J. (2010). The zebrafish genome encodes the largest vertebrate repertoire of functional aquaporins with dual paralogy and substrate specificities similar to mammals. *BMC Evolutionary Biology* **10**, 38.

Uyttebroek, L., Shepherd, I. T., Hubens, G., Timmermans, J.-P. and Van Nassauw, L. (2013). Expression of neuropeptides and anoctamin 1 in the embryonic and adult zebrafish intestine, revealing neuronal subpopulations and ICC-like cells. *Cell. Tissue. Res.* **354**, 355–370.

Uyttebroek, L., Shepherd, I. T., Vanden Berghe, P., Hubens, G., Timmermans, J.-P. and Van Nassauw, L. (2016). The zebrafish mutant lessen: an experimental model for congenital enteric neuropathies. *Neurogastroenterol Motil* **28**, 345–357.

Vergauwen, L., Benoot, D., Blust, R. and Knapen, D. (2010). Long-term warm or cold acclimation elicits a specific transcriptional response and affects energy metabolism in zebrafish. *Comparative Biochemistry and Physiology Part A: Molecular & Integrative Physiology* **157**, 149–157.

Vlachakis, D., Bencurova, E., Papangelopoulos, N. and Kossida, S. (2014). Chapter Seven - Current State-of-the-Art Molecular Dynamics Methods and Applications. In *Advances in Protein Chemistry and Structural Biology* (ed. Donev, R.), pp. 269–313. Academic Press.

Wallace, A. S. and Burns, A. J. (2005). Development of the enteric nervous system, smooth muscle and interstitial cells of Cajal in the human gastrointestinal tract. *Cell Tissue Res* **319**, 367–382.

Wallace, K. N., Akhter, S., Smith, E. M., Lorent, K. and Pack, M. (2005). Intestinal growth and differentiation in zebrafish. *Mech. Dev.* **122**, 157–173.

Wang, X.-Y., Ward, S. M., Gerthoffer, W. T. and Sanders, K. M. (2003). PKC-ϵ translocation in enteric neurons and interstitial cells of Cajal in response to muscarinic stimulation. *Am J Physiol Gastrointest Liver Physiol* **285**, G593–G601.

Wang, Y.-X., Zheng, Y.-M., Mei, Q.-B., Wang, Q.-S., Collier, M. L., Fleischer, S., Xin, H.-B. and Kotlikoff, M. I. (2004). FKBP12.6 and cADPR regulation of Ca2+ release in smooth muscle cells. *Am J Physiol Cell Physiol* **286**, C538–C546.

Ward, S. M., Ördög, T., Bayguinov, J. R., Horowitz, B., Epperson, A., Shen, L., Westphal, H. and Sanders, K. M. (1999). Development of interstitial cells of Cajal and pacemaking in mice lacking enteric nerves. *Gastroenterology* **117**, 584–594.

Ward, S. M., Ördög, T., Koh, S. D., Baker, S. A., Jun, J. Y., Amberg, G., Monaghan, K. and Sanders, K. M. (2000). Pacemaking in interstitial cells of Cajal depends upon calcium handling by endoplasmic reticulum and mitochondria. *J Physiol* **525**, 355–361.

Watanabe, Y. and Dreifus, L. S. (1968). Newer concepts in the genesis of cardiac arrhythmias. *Am Heart J* **76**, 114–135.

Wegener, J. W., Schulla, V., Koller, A., Klugbauer, N., Feil, R. and Hofmann, F. (2006). Control of intestinal motility by the Cav1.2 L-type calcium channel in mice. *The FASEB Journal* **20**, 1260–1262.

Westerfield, M. (2007). *The zebrafish book: a guide for the laboratory use of zebrafish (Danio rerio)*. Univeristy of Oregon.

Won, K.-J., Sanders, K. M. and Ward, S. M. (2005). Interstitial cells of Cajal mediate mechanosensitive responses in the stomach. *Proc Natl Acad Sci U S A* **102**, 14913–14918.

Yamamoto, M. (1977). Electron Microscopic Studies on the Innervation of the Smooth Muscle and the Interstitial Cell of Cajal in the Small Intestine of the Mouse and Bat. *Arch Histol Jap* **40**, 171–201.

Yang, Y. D., Cho, H., Koo, J. Y., Tak, M. H., Cho, Y., Shim, W.-S., Park, S. P., Lee, J., Lee, B., Kim, B.-M., et al. (2008). TMEM16A confers receptor-activated calcium-dependent chloride conductance. *Nature* **455**, 1210–1215.

Ye, L., Bae, M., Cassilly, C. D., Jabba, S. V., Lu, H.-Y., Wang, J., Thompson, J. D., Lickwar, C. R., Poss, K. D., Jordt, S.-E., et al. (2020). Enteroendocrine cells sense bacterial tryptophan catabolites to activate enteric and vagal neuronal pathways. *bioRxiv* 2020.06.09.142133.

Yoneda, S., Fukui, H. and Takaki, M. (2004). Pacemaker activity from submucosal interstitial cells of Cajal drives high-frequency and low-amplitude circular muscle contractions in the mouse proximal colon. *Neurogastroenterol Motil* **16**, 621–627.

Youm, J. B., Zheng, H., Koh, S. D. and Sanders, K. M. (2019). Na-K-2Cl Cotransporter and Store-Operated Ca2+ Entry in Pacemaking by Interstitial Cells of Cajal. *Biophysical Journal* **117**, 767–779.

Yu, K., Jiang, T., Cui, Y., Tajkhorshid, E. and Hartzell, H. C. (2019). A network of phosphatidylinositol 4,5-bisphosphate binding sites regulates gating of the Ca^{2+}-activated Cl^- channel ANO1 (TMEM16A). *Proc Natl Acad Sci USA* **116**, 19952–19962.

Zhang, H., Holden, A. V., Kodama, I., Honjo, H., Lei, M., Varghese, T. and Boyett, M. R. (2000). Mathematical models of action potentials in the periphery and center of the rabbit sinoatrial node. *American Journal of Physiology-Heart and Circulatory Physiology* **279**, H397–H421.

Zheng, H., Park, K. S., Koh, S. D. and Sanders, K. M. (2014). Expression and function of a T-type Ca2+ conductance in interstitial cells of Cajal of the murine small intestine. *Am J Physiol Cell* **306**, C705–C713.

Zheng, H., Drumm, B. T., Zhu, M. H., Xie, Y., O'Driscoll, K. E., Baker, S. A., Perrino, B. A., Koh, S. D. and Sanders, K. M. (2020). Na+/Ca2 + Exchange and Pacemaker Activity of Interstitial Cells of Cajal. *Front Physiol* **11**,.

Zhou, J., Guo, S.-Y., Zhang, Y. and Li, C.-Q. (2014). Human prokinetic drugs promote gastrointestinal motility in zebrafish. *Neurogastroenterol. Motil.* **26**, 589–595.

Zhu, Y., Golden, C. M., Ye, J., Wang, X.-Y., Akbarali, H. I. and Huizinga, J. D. (2003). ERG K+ currents regulate pacemaker activity in ICC. *Am J Physiol Gastrointest Liver Physiol* **285**, G1249–G1258.

Zhu, M. H., Kim, T. W., Ro, S., Yan, W., Ward, S. M., Koh, S. D. and Sanders, K. M. (2009). A Ca2+-activated Cl− conductance in interstitial cells of Cajal linked to slow wave currents and pacemaker activity. *J Physiol* **587**, 4905–4918.

Zhu, M. H., Sung, T. S., Kurahashi, M., O'Kane, L. E., O'Driscoll, K., Koh, S. D. and Sanders, K. M. (2016). Na+-K+-Cl− cotransporter (NKCC) maintains the chloride

gradient to sustain pacemaker activity in interstitial cells of Cajal. *Am J Physiol Gastrointest Liver Physiol* **311**, G1037–G1046.

Vita

Savanna Ciara Sheridan was born in Norfolk, Virginia, to Heidi and Brian Sheridan. She graduated from First Colonial High School in 2014. In Fall 2014, she started at Appalachian State University and studied Biology. In May 2018 she completed her Bachelor of Science in Biology. To continue her education, she attended graduate school at Appalachian State University to earn a Master's of Science degree. The M.S. was awarded in December 2020.